

The star-forming environment of an ultraluminous X-ray source in NGC 4559: an optical study

Roberto Soria,^{1,2★} Mark Cropper,¹ Manfred Pakull,³ Richard Mushotzky⁴
and Kinwah Wu¹

¹*MSSL, University College London, Holmbury St Mary, Surrey RH5 6NT*

²*Harvard-Smithsonian Center for Astrophysics, 60 Garden Street, Cambridge, MA 02138, USA*

³*Observatoire de Strasbourg, 11, rue de l'Université, Strasbourg F-67000, France*

⁴*Laboratory for High Energy Astrophysics, NASA Goddard Space Flight Center, Greenbelt, MD 20771, USA*

Accepted 2004 September 24. Received 2004 September 23; in original form 2004 May 4

ABSTRACT

We have studied the candidate optical counterparts and the stellar population in the star-forming complex around the bright ultraluminous X-ray source (ULX) in the western part of the spiral galaxy NGC 4559, using the *HST* Wide Field Planetary Camera 2 (WFPC2), *XMM-Newton*/Optical Monitor and ground-based data. We find that the ULX is located near a small group of OB stars, but is not associated with any massive young clusters nor with any extraordinary massive stars. The brightest point source in the *Chandra* error circle is consistent with a single blue supergiant (BSG) of mass $\approx 20 M_{\odot}$ and age ≈ 10 Myr. A few other stars are resolved inside the error circle: mostly BSGs and red supergiants (RSGs) with inferred masses ≈ 10 – $15 M_{\odot}$ and ages ≈ 20 Myr. This is consistent with the interpretation of this ULX as a black hole (BH) accreting from a high-mass donor star in its supergiant phase, with mass transfer occurring via Roche-lobe overflow. The observed optical colours and the blue-to-red supergiant ratio suggest a low metal abundance for the stellar population: $0.2 \lesssim Z/Z_{\odot} \lesssim 0.4$ (using the Padua tracks), or $0.05 \lesssim Z/Z_{\odot} \lesssim 0.2$ (using the Geneva tracks). The age of the star-forming complex is $\lesssim 30$ Myr. $H\alpha$ images show that this star-forming region has a ring-like appearance. We propose that it is an expanding wave of star formation, triggered by an initial density perturbation, in a region where the gas was only marginally stable to gravitational collapse. We also suggest that the most likely trigger was a collision with a satellite dwarf galaxy going through the gas-rich outer disc of NGC 4559 less than 30 Myr ago. The culprit could be the dwarf galaxy visible a few arcsec north-west of the complex. If this is the case, this system is a scaled-down version of the Cartwheel galaxy. The X-ray data favour a BH more massive ($M > 50 M_{\odot}$) than typical Milky Way BH candidates. The optical data favour a young BH originating in the recent episode of massive star formation; however, they also rule out an association with young massive star clusters (none are present in the X7 field). We speculate that other mechanisms may lead to the formation of relatively massive BHs (perhaps $M \sim 50$ – $100 M_{\odot}$) from stellar evolution processes in low-metallicity environments, or when star formation is triggered by galactic collisions.

Key words: accretion, accretion discs – black hole physics – galaxies: individual: NGC 4559 – X-rays: galaxies – X-rays: stars.

1 INTRODUCTION

Ultraluminous X-ray sources (ULXs) with apparent (isotropic) luminosities $> 10^{39}$ erg s⁻¹ have been detected in many spiral, irregular and elliptical galaxies; however, most sources brighter than $\approx 5 \times$

10^{39} erg s⁻¹ are located in star-forming galaxies, thus suggesting that they are associated with young populations (Irwin, Bregman & Athey 2004; Swartz et al. 2004). The masses, ages and mechanisms of formation of the accreting objects are still unclear, as is the geometry of emission. For most of the sources, multiband observations so far have not been able to rule out any of the three main competing ULX models, namely intermediate-mass black holes (BHs; Colbert & Mushotzky 1999), normal X-ray binaries with beamed emission

★E-mail: Roberto.Soria@mssl.ucl.ac.uk

(Fabrika & Mescheryakov 2001; King et al. 2001; Körding, Falcke & Markoff 2002), or with super-Eddington emission from inhomogeneous discs (Begelman 2002). These different scenarios also predict different duty cycles and time-scales for the X-ray-bright phases, thus leading to different predictions for the total number of such systems (active or quiescent) in a galaxy. However, in a few cases, such as for the brightest ULX in M 82 (Strohmayer & Mushotzky 2003) and for NGC 4559 X7, the subject of this paper, there is spectral and timing evidence against beaming (Cropper et al. 2004; henceforth, Paper I).

The identification of an optical counterpart can provide important information, complementing the X-ray data. For example, it can help in constraining the age, the mechanism of mass transfer and the mass-transfer rate in the system. X-ray ionized emission nebulae have been found around many ULXs (Pakull & Mirioni 2002; Kaaret, Ward & Zezas 2004): in some cases, they provide strong evidence against the beaming model (e.g. for Holmberg II X-1, Pakull & Mirioni 2002); in other cases, instead, they suggest anisotropic emission (IC 342 X-1, Roberts et al. 2003). The presence of a young, massive star cluster at or near a ULX position (as suggested for the ULXs in the Antennae, Zezas et al. 2002) would be consistent with the formation of an intermediate-mass BH from merger processes in a dense cluster core (Portegies et al. 2004). In some cases, the identification of an optical counterpart has shown that the X-ray source was not a ULX but a background active galactic nucleus (AGN; Masetti et al. 2003). In one other case, a strong limit on the mass of the donor star ($M < 1 M_{\odot}$) suggests that the supposed ULX is instead a foreground AM Her system (Weisskopf et al. 2004). However, in general, unique identifications of ULX optical counterparts have proved difficult, even when *HST* and *Chandra* images are available. In the few cases when reliable stellar identifications have been proposed (NGC 1313 X-2, Zampieri et al. 2004; NGC 5204, Roberts et al. 2001; Liu, Bregman & Seitzer 2004; NGC 3031 X-11, Liu, Bregman & Seitzer 2002), the candidate donor stars have masses $\approx 15\text{--}30 M_{\odot}$.

Located at a distance of ≈ 10 Mpc (Tully 1988; Sanders et al. 2003), the late-type spiral NGC 4559 [Type SAB(rs)cd] hosts three ULXs with isotropic luminosities $\gtrsim 10^{39}$ erg s $^{-1}$; two of them have X-ray luminosities $\gtrsim 10^{40}$ erg s $^{-1}$ (Paper I). Its low foreground Galactic absorption ($n_{\text{H}} \approx 1.5 \times 10^{20}$ cm $^{-2}$; Dickey & Lockman 1990) makes it suitable for X-ray and optical studies aimed at determining the nature of these sources, and their relation with the host environment. A study of the X-ray timing and spectral properties of the two brightest X-ray sources in NGC 4559, based on *XMM-Newton* and *Chandra* data, was presented in Paper I; see also Roberts et al. (2004). Here, we investigate the possible optical counterparts and stellar environment of NGC 4559 X7 (adopting the naming convention of Vogler, Pietsch & Bertoldi 1997 and Paper I). For convenience, its main X-ray properties are also summarized here (Table 1). A study of the optical counterparts and environments of the other bright X-ray sources in this galaxy is left to further work (*HST* Advanced Camera for Surveys (ACS) observations scheduled for 2005 March).

2 OPTICAL OBSERVATIONS

NGC 4559 X7 is located in a relatively isolated region of young star formation at the edge of the Galactic disc, ≈ 2.0 arcmin south-west of the nucleus (Fig. 1). Because our viewing angle is 69° (Tully 1988), this corresponds to a distance $\approx 16d_{10}$ kpc, where d_{10} is the distance to NGC 4559 in units of 10 Mpc. A log of the *Chandra* and *XMM-Newton* observations is given in Paper I. In the optical band,

Table 1. Main X-ray fitting parameters for NGC 4559 X7, for an absorbed blackbody plus power-law model [$\text{WABS}_{\text{Gal}} * \text{tbvarabs} * (\text{bb} + \text{po})$ in XSPEC]. The data are from the *Chandra* and *XMM-Newton* observations of 2001–2003. We list here the isotropic emitted luminosity and the luminosity in the thermal component, in the 0.3–10 keV band, assuming $d = 10$ Mpc and $n_{\text{H,Gal}} = 1.5 \times 10^{20}$ cm $^{-2}$.

Parameter	2001 Jan	2001 Jun	2003 May
$Z (Z_{\odot})$	(0.31) ^(a)	(0.31) ^(a)	$0.31^{+0.27}_{-0.20}$
$n_{\text{H}} (10^{21} \text{ cm}^{-2})$	$3.6^{+0.9}_{-1.1}$	$5.7^{+0.9}_{-1.1}$	$4.3^{+0.9}_{-1.1}$
$kT_{\text{bb}} (\text{keV})$	$0.12^{+0.06}_{-0.06}$	$0.12^{+0.01}_{-0.01}$	$0.12^{+0.01}_{-0.01}$
$K_{\text{bb}} (10^{-5})$	$0.9^{+0.1}_{-0.4}$	$2.3^{+0.5}_{-0.5}$	$0.8^{+0.8}_{-0.4}$
Γ	$1.80^{+0.08}_{-0.08}$	$2.13^{+0.08}_{-0.08}$	$2.23^{+0.06}_{-0.05}$
$K_{\text{po}} (10^{-4})$	$1.8^{+0.2}_{-0.2}$	$2.9^{+0.2}_{-0.2}$	$2.4^{+0.3}_{-0.2}$
$L_{\text{x}} (10^{40} \text{ erg s}^{-1})$	2.0	3.4	2.0
$L_{\text{x}}^{\text{bb}} (10^{40} \text{ erg s}^{-1})$	0.6	1.6	0.5

^aFixed from the *XMM-Newton* value.

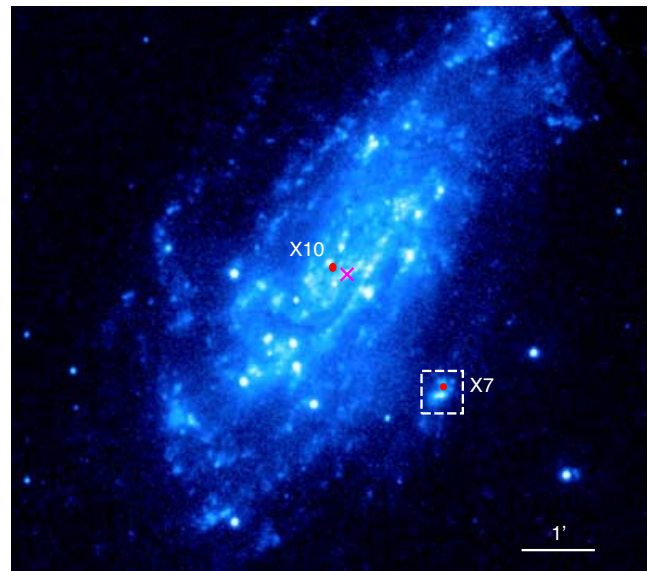


Figure 1. *XMM-Newton* Optical Monitor (OM) image of NGC 4559, in the UVW1 filter. North is up, east is to the left. The locations of the two brightest ($L_{\text{x}} > 10^{40}$ erg s $^{-1}$) X-ray sources are marked with circles and the galactic nucleus (also an X-ray source) with a cross. The area inside the dashed square is shown in more detail in Fig. 2, from the *HST* WFPC2.

the field of NGC 4559 X7 was observed by the *HST* Wide Field Planetary Camera 2 (WFPC2) on 2001 May 25, with a series of four 500-s exposures in each of the three broad-band filters f450w ($\approx B$), f555w ($\approx V$) and f814w ($\approx I$). We retrieved the combined WFPC2 associations as well as the individual exposures from the Multimission Archive at Space Telescope (MAST) public archive.

The X-ray position of X7 is located on the PC chip, in the WFPC2 images. The star-forming complex around the X-ray source is also entirely contained in the PC chip image (Fig. 2). The astrometric registration of the MAST associations has errors $\gtrsim 1$ arcsec (i.e. the same stars have different World Coordinate System (WCS) coordinates in the three combined images). In the absence of bright stars in the PC chip, we used stars from the United States Naval Observatory

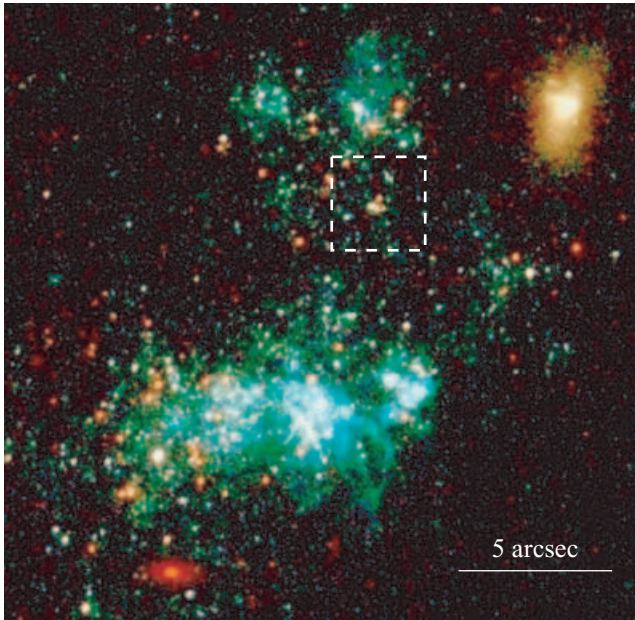


Figure 2. *HST* WFPC2 (PC chip) true-colour image of the field around NGC 4559 X7. North is up, east is to the left. Red, green and blue colours correspond to the f814w, f555w and f450w filters, respectively. Notice the colour difference between the star-forming complex, populated by young massive stars, and the old (yellow) population in the galaxy near the top right corner. The area inside the dashed square is shown in more details in Fig. 3.

(USNO)-B1.0 Catalog (Monet et al. 2003) to correct the relative and absolute astrometric registration of the three images. We estimate that we have thus reduced the astrometric error to <0.4 arcsec for the PC frame. We also applied this new astrometric registration to a mosaiced WFPC2 image, verifying that the error is $\lesssim 0.4$ arcsec in all chips. The *Chandra* astrometry is generally accurate to $\lesssim 0.6$ arcsec. In this case, we verified that the position of the nuclear X-ray source coincides to within ≈ 0.3 arcsec with the position of one of the two nuclear sources in the Two Micron All Sky Survey (2MASS) catalogue. Only two other *Chandra* sources have counterparts in the USNO-B1.0 Catalog: the differences between the X-ray and optical positions are ≈ 0.4 and ≈ 0.2 arcsec. We can therefore take 0.6 arcsec as a conservative upper limit to the *Chandra* astrometric error, and 0.7 arcsec (≈ 34 pc) as the total error when we overlap the X-ray and optical images.

3 DATA ANALYSIS

Before carrying out the photometric analysis, we corrected the WFPC2 images for geometric distortions, multiplying the image files by the standard correction file (f1k155bu.r9h) available from the WFPC2 web site¹ (Gonzaga 2002). We then used DAOPHOT tasks in IRAF to detect stellar sources and measure their brightness.

We have performed a detailed photometric analysis for the sources in the PC chip (1.6×1.6 kpc² field of view at the distance of NGC 4559), which includes the whole star-forming complex around X7. We detected ≈ 260 stars or star-like objects (after rejecting a few extended objects, likely to be background galaxies), at the 4σ level in the f555w-filter image. We also ran the source-finding routine

DAOFIND independently on the f450w and f814w images, and compared the three lists. This did not add any new stellar objects, i.e. there are no stars detected at the 4σ level in either filter that are not also detected in the f555w filter. The significance of detection is, in general, slightly higher in the f555w filter than in the other two; in other words, some of the stars detected at the 4σ level in f555w are only $\approx 3\sigma$ detections in f450w and f814w. Setting the threshold at 3.5σ in the f555w filter or using a combined image in the source-finding routine led to the detection of more stars, but we verified that the additional sources were too faint for any meaningful colour analysis.

We applied the 4σ -detection source list to each filter image, and used PHOT and ALLSTARS to obtain instrumental magnitudes for the point sources in all three filters. Having to deal with a crowded field, we built a point spread function from the brightest, isolated stars and carried out profile-fit photometry rather than simple aperture photometry. The zero-points were taken from Andrew Dolphin's up-to-date tables² (last updated on 2002 September 17; see also Holtzman et al. 1995; Dolphin 2000). We also applied A. Dolphin's equation to carry out the charge-transfer-efficiency corrections. We then applied the colour transformation coefficients listed in A. Dolphin's web site to obtain standard B , V , I colours in addition to the instrumental magnitudes. Finally, we added and tried to detect artificial stars in our images, to determine the completeness limit. We estimate that our sample is complete down to $m_{555} \approx V \approx 24.9$.

Colour-magnitude diagrams of the stars in the X7 field allowed us to study their age and mass distribution. We compared the observed colours with two sets of evolutionary tracks and isochrones for single stars: the Geneva models (Meynet et al. 1994; Lejeune & Schaerer 2001; data files available on VizieR) and the Padua models (Fagotto et al. 1994; Salasnich et al. 2000; Girardi et al. 2002; data files available on VizieR and at <http://pleiadi.pd.astro.it/>). For the Geneva models, we used the e-type grid (enhanced mass loss), which Lejeune & Schaerer (2001) suggest to be preferable for stars of mass $>7 M_{\odot}$. For the Padua models, we used solar scale rather than α -enhanced grids (see Salasnich et al. 2000 for a discussion of this issue). Whenever possible, we compared the observed colours directly with the tracks and isochrones in the WFPC2 photometric system; such models are available for f555w and f814w. However, they are not available for the blue filter f450w: the other, more commonly used blue filter f439w is generally chosen for synthetic models, because it is a closer approximation to the standard B filter. In that case, we compared the $(B, B - V)$ model tracks with the $(B, B - V)$ colours of the observed stars, obtained with Dolphin's transformation coefficients, as mentioned above. To convert the theoretical stellar tracks from absolute to apparent magnitudes, we assumed a distance modulus $d_M = 30.0$ mag (corresponding to a distance of 10 Mpc) throughout our analysis. We also corrected the theoretical tracks for the line-of-sight Galactic extinction $E(B - V) = 0.018$ (Schlegel, Finkbeiner & Davis 1998).

We are aware that all the available sets of evolutionary tracks and isochrones are calculated for single stars, while most O stars come in double or triple systems. Besides, some of the bright data points in our colour-magnitude diagrams may in fact refer to a superposition of two or more fainter, unresolved stars. These are well-known limitations of stellar population studies. None the less, similar studies carried out for nearby galaxies have generally given a reliable view of the stellar population properties.

¹ <http://www.stsci.edu/instruments/wfpc2>

² http://www.noao.edu/staff/dolphin/wfpc2_calib/

Table 2. Standard magnitudes of the brightest stars detected within 1 arcsec from the ULX position.

No.	<i>B</i> brightness	<i>V</i> brightness	<i>I</i> brightness
1	22.85 ± 0.16	23.03 ± 0.12	23.05 ± 0.12
2	24.25 ± 0.24	23.73 ± 0.16	22.87 ± 0.16
3	25.18 ± 0.24	24.27 ± 0.14	22.99 ± 0.14
4	25.09 ± 0.25	24.50 ± 0.13	23.89 ± 0.16
5	25.17 ± 0.22	25.43 ± 0.19	25.38 ± 0.48
6	25.45 ± 0.25	25.33 ± 0.17	25.05 ± 0.33
7		(Falling on a hot pixel)	
8	23.68 ± 0.12	24.00 ± 0.14	24.05 ± 0.18

4 STELLAR POPULATION IN THE ULX FIELD

4.1 Overview

We divide our analysis into two parts. First (Sections 4.2, 4.3), we shall discuss the general properties of the stellar population in the star-forming complex (metal abundance, characteristic masses and ages). Then (Sections 4.4, 4.5), we shall focus on the brightest stars detected within 1 arcsec from the X-ray position of the X7 ULX, discussing whether any of them can be the donor stars for the accreting BH.

The brightness in the standard system of the candidate X7 counterparts is listed in Table 2; the numbers correspond to those overplotted in Fig. 3. The same set of stars has been plotted with their respective error bars in all colour–magnitude diagrams throughout this section (Figs 4, 5, 6, 9 and 10), to be more easily identified and to provide an indication of typical photometric errors at various brightnesses and colours.

4.2 Metal abundance

The first apparent result (independent of the choice of comparison models) from the observed optical colour distribution of the stars

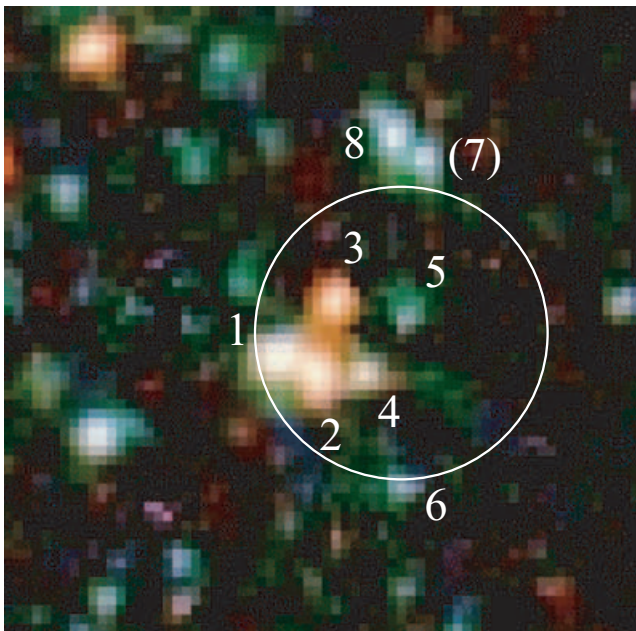


Figure 3. Close-up view of the immediate environment of X7. The ULX is located inside a circle with 0.7 arcsec radius (this combines the error in the *Chandra* pointing accuracy and that in the *HST* WFPC2 astrometry). The brightness of the labelled stars around X7 is listed in Table 2.

from the whole star-forming complex is the clear separation between two groups of blue and red stars (Fig. 4). The latter ($m_{555} - m_{814} \gtrsim 0.7$) are easily identified as red supergiants (RSGs; stars with shell hydrogen or, later, shell Helium burning); we find 46 of them. The blue stars comprise blue supergiants (BSGs; stars in their core-Helium-burning phase of evolution) and massive stars ($M \gtrsim 15 M_{\odot}$) slightly evolved but still on the main sequence (MS). An unequivocal separation between these two classes of bright blue stars in a stellar population is usually difficult (Dohm-Palmer & Skillman 2002). Using a colour-index histogram of Sextans A stars with absolute magnitude $-5.6 < M_V < -3.2$, Dohm-Palmer & Skillman (2002) showed that, although there is some overlapping, most of the stars with $(V - I)_0 < -0.13$ are MS stars and most of those with $(V - I)_0 > -0.13$ are BSG. This dividing line is independent of M_V . They also found approximately the same relative contribution from the two populations in that magnitude range.

NGC 4559 is 7 times further away than Sextans A, so our detection limit is at $M_V \approx -5$ and there is a higher chance of confusion. At magnitudes $M_V < -5$, separating between the two subgroups of blue stars is less straightforward (see fig. 2 in Dohm-Palmer & Skillman 2002). If we assume that the dividing line found by Dohm-Palmer & Skillman (2002) also applies to our sample, i.e. if we identify as MS all the stars bluer than $(V - I)_0 = -0.13$, corresponding to an observed colour index $m_{555} - m_{814} \approx -0.10$, we obtain (Fig. 5) that $\approx \frac{2}{3}$ of the blue stars in the X7 field are BSG (i.e. ≈ 140). We can conservatively conclude that ≈ 100 – 150 stars are BSG and ≈ 40 – 50 are RSG.

Hence, we estimate a blue-to-red supergiant ratio $\approx 3 \pm 1$, similar to the values observed in metal-poor galaxies such as the Small Magellanic Cloud (SMC; Langer & Maeder 1995) or Sextans A (Dohm-Palmer & Skillman 2002). This ratio is 1 order of magnitude higher in metal-rich environments, at solar abundance or higher (Langer & Maeder 1995). The metal dependence in the evolutionary tracks of massive stars has been explained (Maeder & Meynet 2001) as an effect of rotation: metal-poor stars lose less mass and angular momentum in a wind, are more likely to be fast rotators (close to their break-up speed), end their H-burning phase with higher He-core masses and expand to much larger radii. (For recent studies and reviews of the blue-to-red supergiant ratio, see Langer & Maeder 1995; Salasnich, Bressan & Chiosi 1999; Maeder & Meynet 2001; Guo & Li 2002).

Another indication of the metal-poor nature of the stellar population in the X7 field comes directly from the colours of the RSG population (Figs 4, 6 and 7). For a fixed metal abundance, the colour indices predicted by the Geneva and Padua tracks differ by ~ 0.5 – 1 mag (Fig. 7), with the Geneva tracks systematically redder. However, both sets of models indicate a subsolar metallicity: $0.2 \lesssim Z/Z_{\odot} \lesssim 0.4$ (Padua), or $0.05 \lesssim Z/Z_{\odot} \lesssim 0.2$ (Geneva).

In conclusion, both the blue-to-red supergiant ratio and the RSG colour indices point to a low metal abundance, similar to values found in the SMC and in other nearby dwarf galaxies. An association between ULXs and metal-poor environments was suggested by Pakull & Mirioni (2002). This is also consistent with the abundance $Z/Z_{\odot} = 0.3^{+0.3}_{-0.2}$ inferred from the X-ray spectral fits to the X7 ULX (Table 1 and Paper I).

4.3 Masses and ages

Various differences between the Geneva and Padua models have been extensively discussed in the literature (e.g. Fioc & Rocca-Volmerange 1997; Lejeune & Buser 1999; Westera et al. 2002). It is well known that, for a given metal abundance, the Geneva tracks for

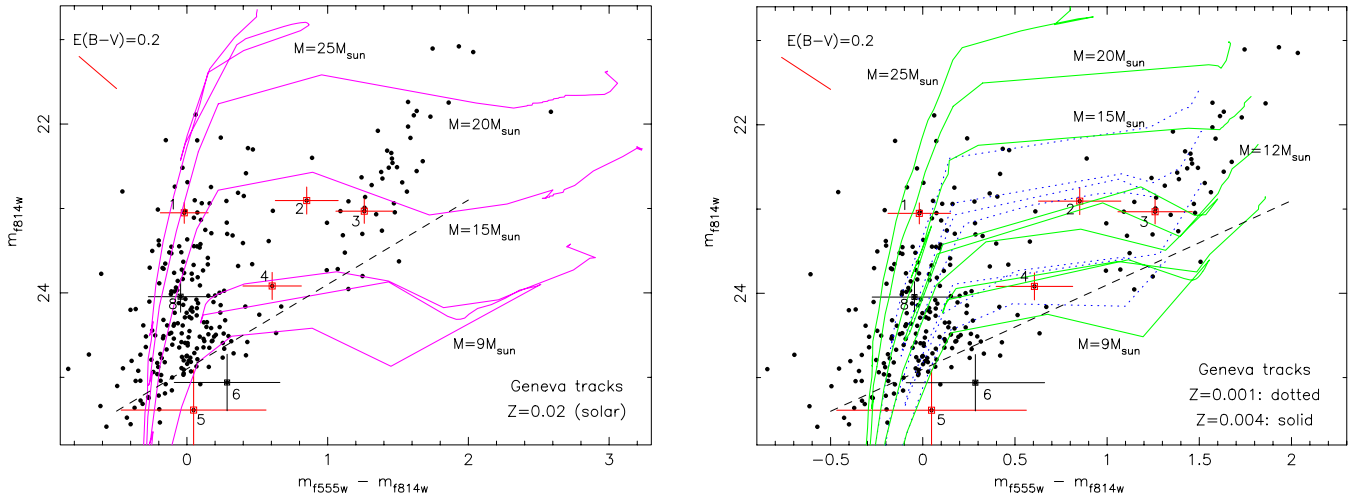


Figure 4. Colour–magnitude diagrams of the stars in the young complex around X7 (the region shown in Fig. 2), in the (f555w, f814w) WPC2 filter system ($\approx(V, I)$), and evolutionary tracks for single stars of various initial masses and metallicities (Geneva tracks). The stars plotted with error bars and number labels are the candidate optical counterparts of the ULX: see Table 2, Fig. 3 and Section 4.4. The tracks have already been corrected for line-of-sight reddening. The bar near the top left corner shows the effect on the data of an (arbitrary) intrinsic reddening $E(B - V) = 0.2$. The dashed black line is the completeness limit of our sample. Left panel: solar abundances are ruled out by the small colour separation observed between the main sequence/blue supergiant (MS/BSG) clump and the red supergiant (RSG) clump (only $(V - I) \approx 1.5$ mag, instead of $(V - I) \approx 2.5$ mag as expected for solar metallicity). Right panel: the Geneva tracks providing the best model for the observed stellar distribution are those for metal abundances $0.001 \lesssim Z \lesssim 0.004$, consistent with the low abundance inferred from the X-ray data. In this panel, we have plotted evolutionary tracks for initial masses of 9, 12 and 15 M_{\odot} at $Z = 0.001$ (dotted lines), and tracks for initial masses of 9, 12, 15, 20 and 25 M_{\odot} at $Z = 0.004$ (solid lines).

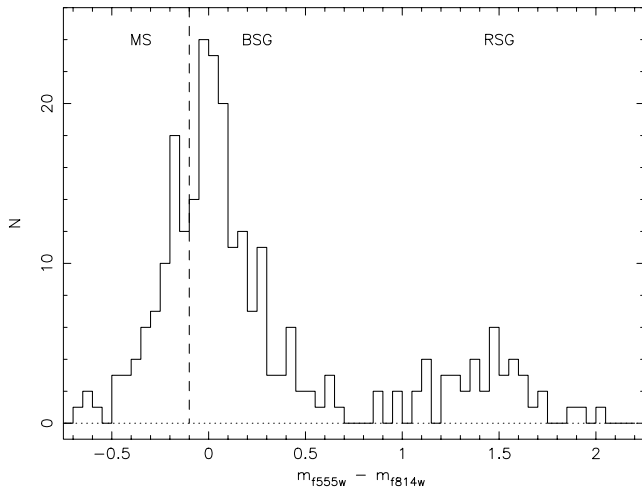


Figure 5. Colour histogram of the stars in the X7 field, showing two separate groups of blue (MS = main sequence and BSGs = blue supergiants) and red stars (RSGs = red supergiants). We cannot separate the MS and BSG populations; however, following Dohm-Palmer & Skillman (2002), we estimate that the stars to the left of the vertical dashed line are more likely to be MS and those to the right BSG.

the red giant and supergiant phases tend to be redder than observed, and the Padua tracks tend to be bluer, especially at low metallicities; or alternatively, that the Geneva tracks predict systematically lower metal abundances than the Padua tracks. This is also evident for example from Fig. 7.

For the stellar population in the X7 field, both the Geneva and the Padua tracks suggest that most of the RSGs have masses ≈ 12 – $14 M_{\odot}$ (Figs 4, 6 and 7), with only a few more massive ones, up to $M \approx 20 M_{\odot}$. On the blue side of the colour–magnitude diagrams,

there is evidence for stars with masses $\approx 25 M_{\odot}$ near the end of their MS phase or in the BSG stage.

The largest number of RSGs are located at $23.9 \lesssim V \lesssim 24.3$ (Fig. 8), corresponding to stars with initial masses $\approx 12 M_{\odot}$. A decreasing number of RSGs is found at fainter V brightnesses (corresponding to lower masses). This is not an effect of incompleteness, because our source list is complete down to $V \approx 24.9$. Indeed, the number of detected blue stars (MS plus BSG) increases at fainter brightness intervals, down to the completeness limit, as expected (Fig. 8). The peak in the RSG distribution at $V \approx 24.1$ is likely the result of the young age of the population: stars with masses $\lesssim 10 M_{\odot}$ have not yet evolved to the RSG stage.

We estimated the dominant age of the population by overplotting the Geneva and Padua theoretical isochrones, for various metal abundances (Figs 9 and 10). We find that the median age of the stars is ≈ 15 – 20 Myr, depending on the choice of model and metal abundance. A few bright, blue stars could be as young as ≈ 3 Myr. The brightness distribution of the RSGs suggests that star formation was much reduced at ages $\gtrsim 30$ Myr. In fact, the integrated colour of the whole star-forming complex (rather blue, with $B - I \approx 0.0$) suggests that, if there is an older, underlying stellar population, its contribution is negligible.

A visual inspection of the stellar colours in Fig. 2 suggests that the main star-forming region south of the X7 ULX does not have a uniform population: most of the RSGs are located on the eastern side, and most of the blue stars and gas are on the western side. To estimate a possible age gradient more quantitatively, we divided this region into two halves: an eastern and a western region containing 88 and 89 stars, respectively. Overplotting the Geneva isochrones on to their colour–magnitude diagram (Fig. 11, left panel), we find that the stellar population in the eastern part of the complex is consistent with a narrow age range (≈ 16 – 18 Myr), with only a few stars as old as ≈ 30 Myr and no stars younger than ≈ 10 Myr. In the western region, instead, we find both young, bright BSGs and MS stars

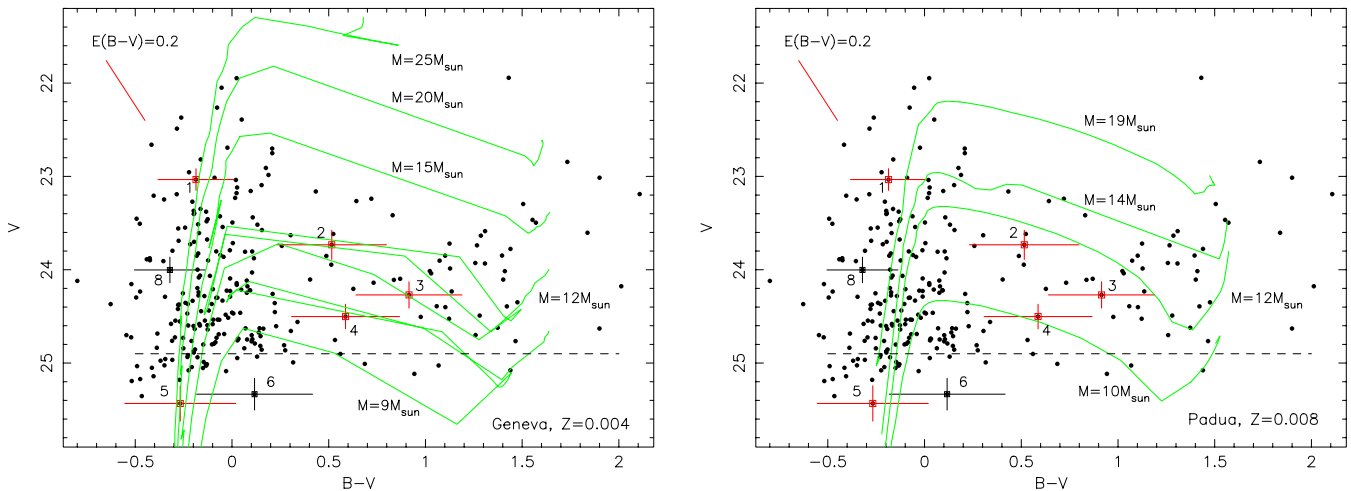


Figure 6. Colour–magnitude diagrams of the stars in the X7 field, in the standard (B, V) system, and evolutionary tracks for single stars of various initial masses. Left panel: tracks from the Geneva models; right panel: tracks from the Padua models. Error bars and labels have the same meaning as in Fig. 4.

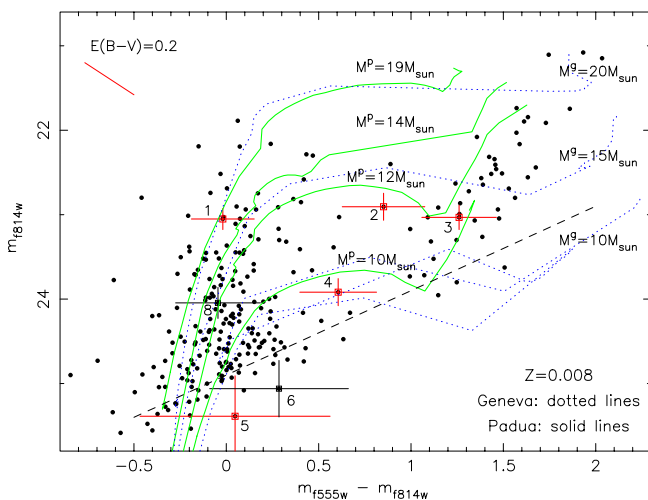


Figure 7. Colour–magnitude diagram in the ($f555w, f814w$) WFPC2 filter system, illustrating the comparison between Geneva and Padua tracks. At a fixed metal abundance, tracks from the Geneva models (dotted lines) are systematically redder than tracks from the Padua model (solid lines). Error bars and symbols are the same as in Fig. 4.

with an age ≈ 3 –10 Myr, and fainter, blue stars, apparently BSGs older than ≈ 25 Myr and with masses $\lesssim 10 M_{\odot}$. The large error in their colours prevents an accurate age determination for this fainter group. It is puzzling to find so many BSGs in that age and mass range without a corresponding number of RSGs. However, these stars are mostly located in a gas-rich area, where we expect a local extinction larger than the Galactic line-of-sight value. We think that these apparently older stars are in fact young but simply more reddened. Sample reddening bars are plotted in the top left corner of all colour–magnitude diagrams (Figs 4, 6, 7 and 9–12).

Star formation in the X7 field probably proceeded through successive bursts, igniting different parts of the complex at different times. In particular, over the last 20 Myr, star formation seems to have propagated from the south-eastern corner of the complex towards the west. A similar analysis for the rest of the X7 field (including the smaller star-forming complex north of the ULX) reveals an

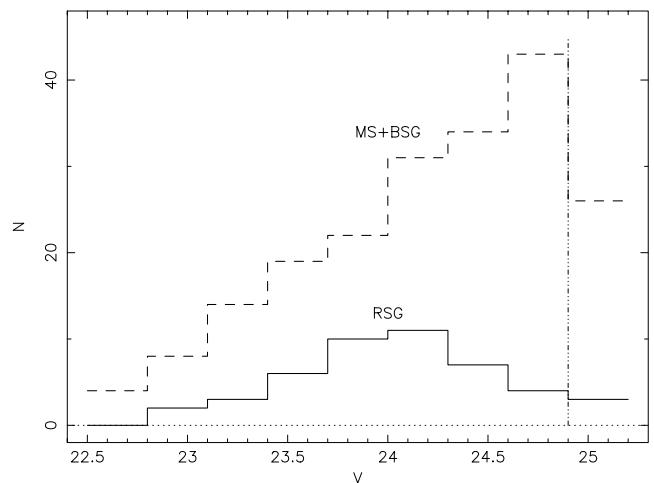


Figure 8. V brightness histogram of the stars in the X7 field, showing that most red supergiants (RSGs) are located at $V \approx 24$. From this, we infer a characteristic age for the recent star formation in the region (see text). The vertical dash-dotted line is the completeness limit.

age distribution of ≈ 10 –20 Myr (Fig. 11, right panel), intermediate between those of the two halves of the southern complex.

There is only one moderately large star cluster in the field, located at RA (2000) = $12^{\text{h}} 35^{\text{m}} 52^{\text{s}}.32$, Dec. (2000) = $+27^{\circ} 55' 55''.1$, i.e. ≈ 12 arcsec (≈ 570 pc) south-east of the ULX. It is unresolved in the PC images (full-width half maximum of its radial profile ≈ 1.7 pixels, similar to all other point sources in the field), hence its size is $\lesssim 3.5$ pc. Its apparent brightness is $B = (20.65 \pm 0.14)$, $V = (20.49 \pm 0.10)$, $I = (19.96 \pm 0.11)$, hence $M_V \approx -9.5$: we have of course excluded it from our colour–magnitude diagrams. From its optical colours and brightness, using the Starburst99 tables (Leitherer et al. 1999) for the case of instantaneous burst, Salpeter initial mass function (IMF), lower stellar-mass limit of $1 M_{\odot}$ and upper stellar-mass limit of $100 M_{\odot}$, we infer an age of 25 ± 5 Myr and a mass $\approx 10^{4.2} M_{\odot}$. Such a cluster would have contained ≈ 70 O stars at its birth and would have today a supernova rate of ≈ 1 – $2 \times 10^{-5} \text{ yr}^{-1}$. If we assumed instead a lower mass limit of $0.1 M_{\odot}$, the total stellar mass in the cluster would be $\approx 10^{4.7} M_{\odot}$.

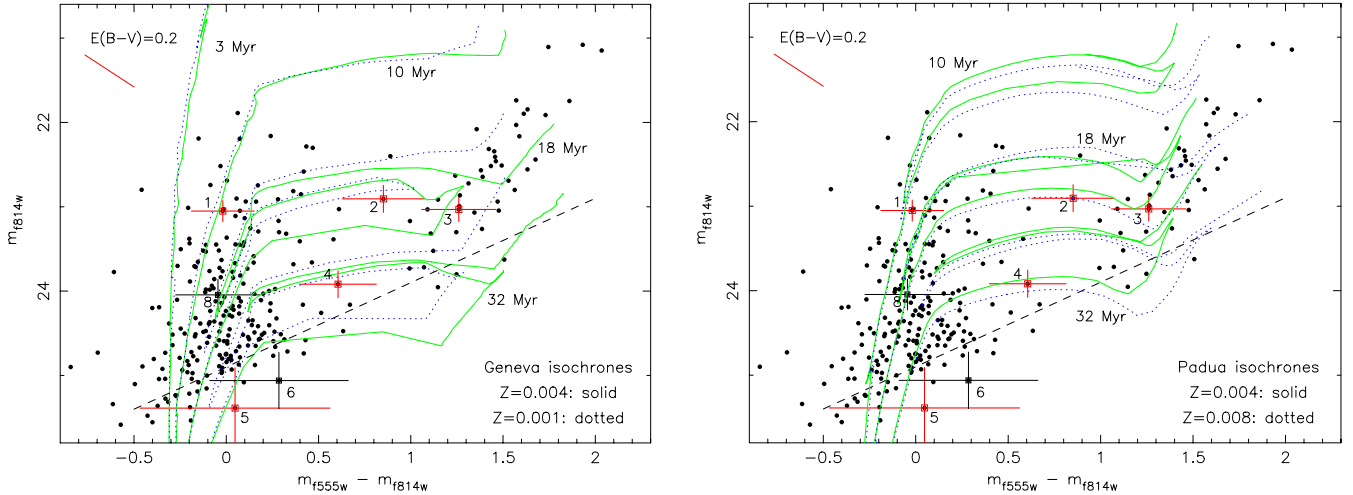


Figure 9. Theoretical isochrones in the $(f555w-f814w, f814w)$ plane, for different choices of metal abundances. Left panels: Geneva models; right panel: Padua models. The labels and error bars have the same meaning as in Fig. 4.

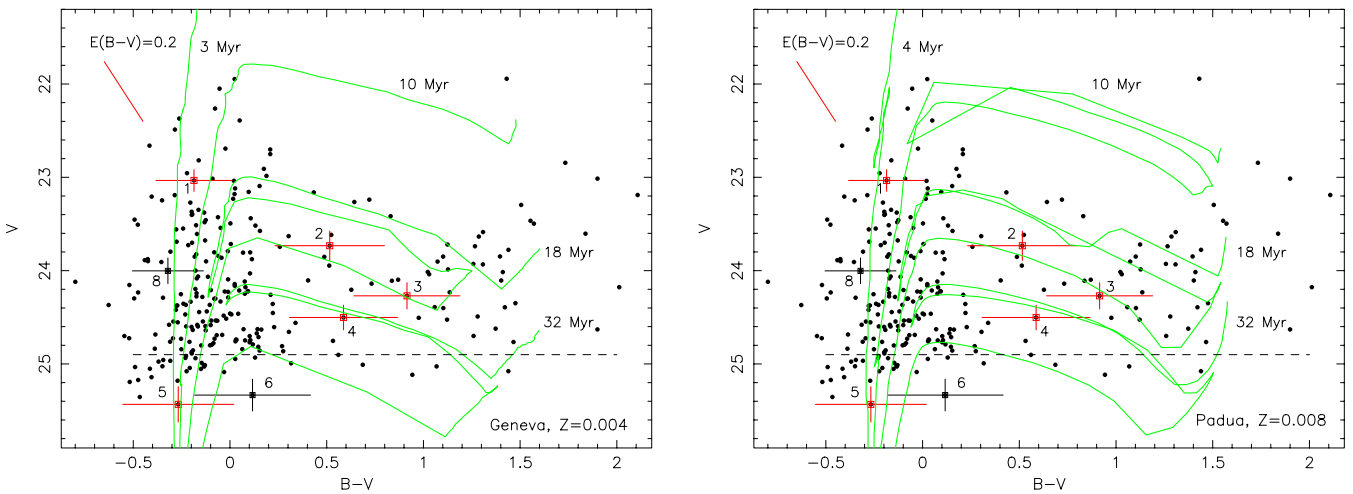


Figure 10. Theoretical isochrones in the $(B-V, V)$ plane. Left panel: Geneva models for $Z = 0.004$; right panel: Padua models for $Z = 0.008$. Symbols and labels as in Fig. 4.

The mass threshold below which the IMF flattens or turns over is still a matter of debate: it is generally estimated that the IMF flattens for $M \lesssim 0.5 M_{\odot}$ (Kroupa, Tout & Gilmore 1990, 1993; Kroupa 2002a) and probably at higher masses in low-metallicity environments such as the Magellanic Clouds (Larson 1998; Kroupa 2001, 2002b). We note that young star clusters with a top-heavy IMF (truncated at a lower mass $\approx 1-3 M_{\odot}$) have been observed in the starburst galaxy M 82, where star formation was probably triggered by tidal interactions (Smith & Gallagher 2001; McCrady, Gilbert & Graham 2003; see also Elmegreen & Shadmehri 2003). Hence, we shall take $M = 1 M_{\odot}$ as an order-of-magnitude approximation for the lower cut-off mass.

4.4 Nature of the donor star

After discussing the general properties of the starburst complex, we now focus on the immediate environment of the ULX. Four point-like sources are detected with signal-to-noise $> 4\sigma$ in the $f555w$ -filter image, inside a 0.7-arcsec error circle centred on the *Chandra* position for X7 (Fig. 3); a fifth star is detected with signal-to-noise

$\approx 3.5\sigma$. We also considered three other bright stars just outside the error circle, at a distance $d < 1$ arcsec from the *Chandra* position. See Fig. 3 and Table 2 for the location and brightness of these stars. (One of them, star no. 7, falls on to a hot WFPC2 pixel:³ it was not possible to derive an accurate brightness.) In our colour-magnitude diagrams (Figs 4, 6, 7, 9, 10 and 12), the five stars plotted with red error bars are those located at < 0.7 arcsec from the X-ray position of the ULX, while the two stars with black error bars are those located at $0.7 \text{ arcsec} < d < 1$ arcsec.

There are clearly many more lower-mass stars in the same region and immediately outside the error circle (Fig. 3), but they are either too faint, or too close to much brighter stars to allow for a meaningful photometric study. The young age of the population implies that all B3 or later-type stars ($M \lesssim 9 M_{\odot}$) are still on the MS. We assume for this work that the true ULX counterpart is one of the more massive stars. However, we cannot rule out the possibility that the true ULX

³ For a list of hot *HST* WFPC2 pixels at various epochs and a general discussion of this problem, see http://www.stsci.edu/instruments/wfpc2/wfpc2_hotpix.html

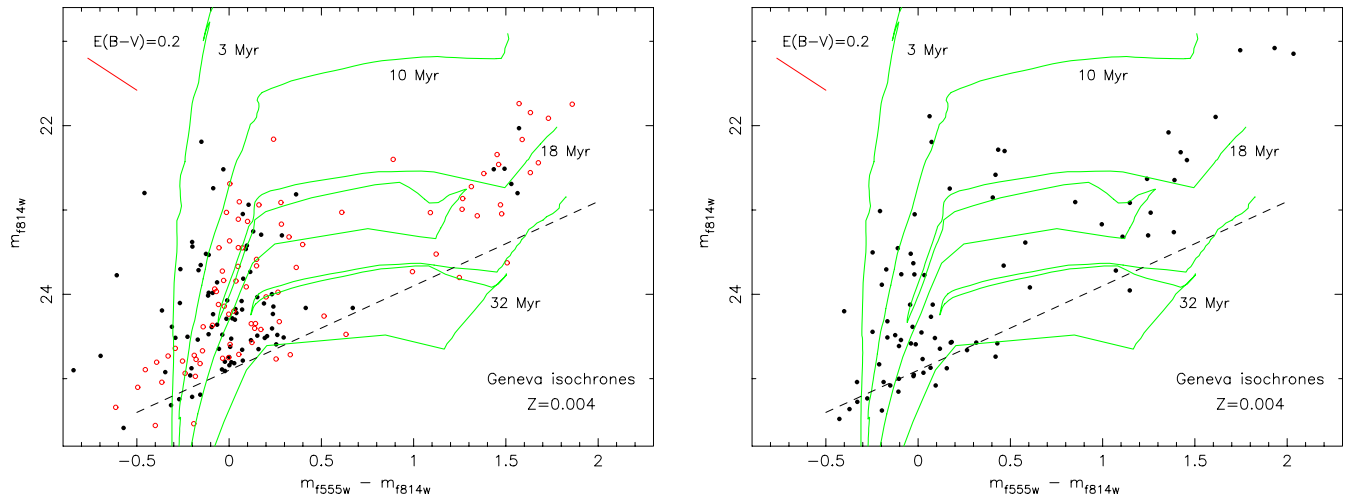


Figure 11. Colour magnitude diagrams for three separate regions in the X7 field, showing age differences in the dominant population (also apparent from the different colours in Fig. 2). Left panel: the south-eastern sector of the star-forming complex shows a narrow age range around 18 Myr (open circles), with no stars younger than ≈ 10 Myr; the south-western sector has a younger population (filled circles), with ongoing star formation and fewer red supergiants (RSGs). Right panel: stellar population in the rest of the X7 field (including, among others, the candidate optical counterparts in the ULX error circle), showing an intermediate age spread, up to an age ≈ 25 Myr.

counterpart is one of the unresolved lower-mass stars, transferring mass via Roche lobe overflow on their nuclear evolution time-scale.

Among the five stars resolved inside the 0.7-arcsec error circle, star no. 1 (Fig. 3) is the brightest in the V band. From the Geneva models, its colours are consistent with a zero-age mass of ≈ 15 – $30 M_{\odot}$ (Figs 4, 6, 7) and an apparent age of ≈ 10 Myr (Figs 9 and 10); it is likely to be in its BSG phase. If this is the case, we infer a bolometric luminosity $\approx 1.4 \pm 0.2 \times 10^5 L_{\odot}$ and an effective temperature $\approx 16\,000 \pm 5000$ K.⁴

The three stars labelled as nos 2, 3 and 4 (Fig. 3) have initial masses ≈ 10 – $12 M_{\odot}$, typical of early-type stars (B0–B2 types when on the MS); with an age of ≈ 20 – 30 Myr, they have already left the MS. One is clearly an RSG, another is a BSG, the third one may be on the blue loop between the BSG and RSG phases. Because of the large uncertainty in the photometry, we cannot constrain the age and mass of star no. 5.

The bright stars around the ULX position appear to be part of a single group; hence, it is possible that they were formed at approximately the same epoch. We find that the Geneva isochrone for an age of 22 Myr and a metal abundance $Z = 0.004$ is consistent (within 1σ) with six of the seven stars (Fig. 12). If we impose this strict age condition, we can also obtain a strong constraint on their masses: they would all be in a narrow range between ≈ 10.5 and $11 M_{\odot}$, with star no. 5 being the least massive. Only star no. 1 appears too blue and too bright (and therefore too massive) to be consistent with an age of 22 Myr. This star is also our strongest candidate for the X7 donor star, given its high mass-loss rate in its BSG stage. If it is indeed the donor star and if we assume that it was also formed at the same epoch as the other stars in the group, we speculate by analogy with typical high-mass X-ray binaries [e.g. LMC X-3, Soria et al. 2001] that its blue colours may be the result of X-ray irradiation.

The fraction of radiation intercepted by the companion star in an X-ray binary is $\approx (R_2/2a)^2$, where R_2 is the radius of the star and the

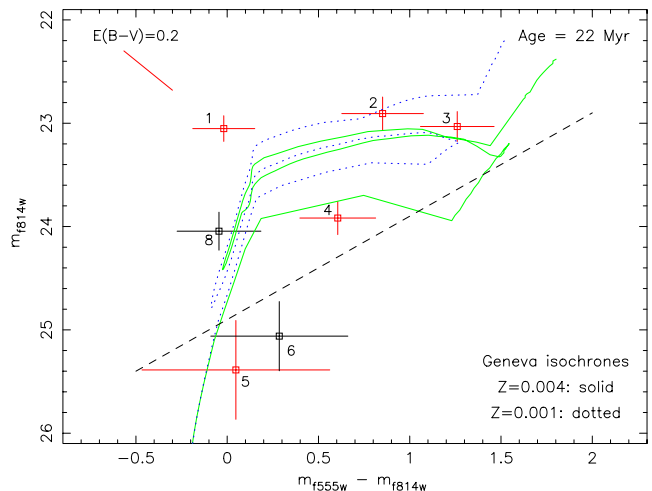


Figure 12. Colour–magnitude diagram and Geneva isochrones for seven candidate optical counterparts of the X7 ULX. An age ≈ 22 Myr is consistent (within 1σ) with six out of seven, for $Z = 0.004$. The initial-mass spread along this isochrone is from $\approx 10.5 M_{\odot}$ (near the location of star no. 5) to $\approx 11.1 M_{\odot}$ (near the location of the red supergiant (RSG) stars nos 2 and 3).

binary separation $a = 2.9 \times 10^{11} M_1^{1/3} (1+q)^{1/3} P_d^{2/3}$ cm (Newton 1687). Here M_1 is the BH mass in solar units, $q = M_2/M_1$ and P_d is the binary period in days. If the donor star is filling its Roche lobe, or is very close to filling it, we can approximate $R_2/a \approx r_L(q) = (0.49q^{2/3})/[0.6q^{2/3} + \ln(1+q^{1/3})]$ (Eggleton 1983). Taking $M_1 \approx 100 M_{\odot}$ and $M_2 \approx 12$ – $25 M_{\odot}$, and assuming isotropic emission, the intercepted X-ray luminosity is ~ 2 – 6×10^{38} erg s⁻¹ (Paper I), to be partly reflected and partly thermalized and re-radiated in the optical/UV bands. The intercepted flux depends of course on the geometry of emission: it will be lower than the values estimated above if the X-ray emission is beamed in the direction normal to the orbital plane. However, it is possible that the intercepted flux is at least of the same order of magnitude as the intrinsic emission from the star ($L_{\text{bol}} \approx 2$ – 5×10^{38} erg s⁻¹ in the BSG phase), causing

⁴ Hence, we note only as an aside that this star is similar to the BSG progenitor of SN 1987A; Podsiadlowski (1992).

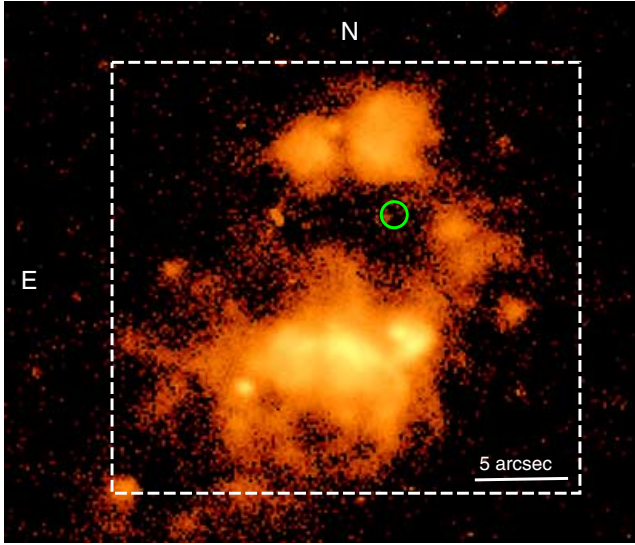


Figure 13. $H\alpha$ image from the 3.6-m CFHT. The $H\alpha$ contour lines for the region inside the dashed box are shown in Fig. 14.

the star to appear bluer and brighter than an isolated star of the same mass and age. There is of course no firm evidence yet for this scenario, so ours is only a speculation, at this stage.

Another piece of evidence in favour of star no. 1 as the true optical counterpart comes from a 1200-s continuum-subtracted $H\alpha$ image (Fig. 13) taken by M. Pakull & L. Mirioni with the 3.6-m Canada–France–Hawaii Telescope (CFHT), on 2000 March 11. Although it has lower spatial resolution than the *HST* WFPC2 images, it clearly reveals line emission associated with star no. 1. The image was not flux calibrated, hence we cannot measure the emitted $H\alpha$ flux precisely. However, we shall give an order-of-magnitude estimate in Section 5.2. Detection of $H\alpha$ emission alone does not of course prove that star no. 1 is the ULX counterpart. We shall discuss possible scenarios for Balmer line emission in Section 5.2, some of them related to accretion or outflows near the compact object in an X-ray binary, some unrelated (e.g. colliding winds, winds from O-type supergiants, discs around Oe/Be stars).

Finally, we searched for possible optical variabilities in each of the five candidate stars. Each *HST* WFPC2 observation was in fact a series of four consecutive 500-s exposures: we looked at the individual frames, but found no variability for any of the possible optical counterparts. Ellipsoidal modulations with an amplitude ≈ 0.2 mag are expected from such systems (in analogy with, for example, the B-type optical counterpart of LMC X-3, Kuiper, van Paradijs & van der Klis 1988); the amplitude could be higher if X-ray irradiation effects on the surface of the companion star are also important. Detection of such modulations is well within the capabilities of the WFPC2 or the ACS on board *HST*. A series of exposures over a longer period of time (a few days) is needed to investigate this possibility, which would strongly constrain the binary period.

4.5 Mass transfer in the ULX

The observed X-ray luminosity of NGC 4559 X7 (Paper I) implies an accretion rate on to the BH of $\approx 3.5\text{--}5 \times 10^{-6} M_{\odot} \text{ yr}^{-1}$, assuming isotropic emission and an efficiency ≈ 0.1 . If the bolometric luminosity is considered, an accretion rate $\gtrsim 10^{-5} M_{\odot} \text{ yr}^{-1}$ is required.

Massive supergiant stars are in an evolutionary phase at which a strong stellar wind drives a large mass loss. If star no. 1 has a

mass $\approx 20\text{--}25 M_{\odot}$, its mass-loss rate in the stellar wind is $\approx 1\text{--}2 \times 10^{-6} M_{\odot} \text{ yr}^{-1}$ ($\sim 10^{20} \text{ g s}^{-1}$) in the BSG stage (Lejeune & Schaerer 2001). This rate is sustained for a time-scale $\approx 5 \times 10^5 \text{ yr}$. As the star evolves towards the RSG stage, the mass-loss rate in the wind will eventually increase to $\approx 10^{-5} M_{\odot} \text{ yr}^{-1}$ for a time-scale of $\approx 10^5 \text{ yr}$. If the donor star is close to filling its Roche lobe, the stellar wind is focused and as a consequence almost all the wind material will be accreted on to the BH; this situation occurs for example in the Galactic source Cyg X-1 (Tarasov, Brocksopp & Lyuty 2003). Such rates of mass transfer in a focussed wind can produce X-ray luminosities typical of moderately bright ULXs. However, the mass-loss rate expected from star no. 1 is not sufficient to explain the isotropic luminosity of NGC 4559 X7. Moreover, a stellar wind is certainly not strong enough to account for the observed luminosity if the donor star in the X7 system has a mass $\approx 10\text{--}15 M_{\odot}$.

A higher accretion rate can be obtained if the donor is directly overflowing its Roche lobe (e.g. Wellstein, Langer & Braun 2001; Vanbeveren, De Loore & Van Rensbergen 1998). In this case, all the mass lost from the donor star will be captured by the BH. The BH candidate LMC X-3 is an example of an X-ray binary containing an early-type star transferring mass on to a (slightly) more massive BH via Roche lobe overflow (e.g. Wu et al. 2001). For a $\sim 20 M_{\odot}$ star, peak mass transfer rates of $\sim 10^{-4} M_{\odot} \text{ yr}^{-1}$ can be achieved, over a thermal time-scale $\sim 10^5 \text{ yr}$ (Wellstein et al. 2001; Podsiadlowski, Rappaport & Han 2003). A proper determination of the accretion rate requires a study of the stability criteria for mass transfer as a function of mass ratio, evolutionary stage of the donor star and rate of loss of angular momentum in a stellar or disc wind (Ritter 1988; Wu 1997). The stability and duration of mass transfer in turn affect the lifetime of the X-ray phase, the mass transfer duty cycle, and the long- and short-term X-ray variabilities, and determine the relative abundance of active ULXs observable in young stellar environments at any given time.

We leave a quantitative investigation of the physical conditions for stable Roche-lobe mass transfer in ULXs, for a range of possible mass ratios, to a follow-up paper. Here we simply point out one phenomenon that may be significant for our understanding of mass transfer in ULXs. In a binary system where mass is transferred from the less massive to the more massive component (as we suppose being the case for most ULXs and in particular for NGC 4559 X7), the orbit widens and therefore the Roche lobe of the donor star expands. If the donor is an MS or subgiant star, its adiabatic mass–radius exponent is > 0 , i.e. its thermal equilibrium radius decreases as the star loses mass. Hence, the star will soon become detached from its Roche lobe and mass transfer will cease, until contact is regained. A loss of angular momentum from the system (for example through a wind) is required to counteract this effect and shrink the orbit, thus ensuring a steady mass transfer. However, if the donor is a supergiant star, its mass–radius exponent is < 0 , so its thermal equilibrium radius will increase as the star loses mass (Wellstein et al. 2001). Hence, a supergiant donor may remain in contact with its Roche lobe and keep transferring mass steadily on to a more massive BH at a high rate, throughout its lifetime (up to $\sim 10^6 \text{ yr}$), even in the absence of angular momentum losses. Thus, we speculate that an O- or B-type supergiant star transferring mass via Roche-lobe overflow on to a more massive BH could be a natural explanation for persistent ULXs. Incidentally, this argument also suggests that the optical counterpart of X7 is more likely to be one of the supergiant stars listed in Table 2, rather than any of the fainter MS stars in the same field.

Finally, although we cannot yet identify the donor star, we can rule out an association of the ULX with a young, massive cluster.

There is a small group of young stars but no bright clusters inside the X-ray error circle (Fig. 3): all the optical sources are consistent with single stars or, at most, the superposition of a few stars. The only moderately large cluster in the field is located $\gtrsim 570$ pc away (projected distance, without considering the viewing angle), on the south-eastern side of the star-forming complex. Given the age of the cluster, a physical association would require an ejection speed $\gtrsim 25 \text{ km s}^{-1}$ for the ULX binary system. This value is too large to be consistent with an intermediate-mass BH (Zezas & Fabbiano 2002).

5 ORIGIN OF THE LARGE STAR-FORMING COMPLEX

5.1 Mass, density and star formation rate in the region

The CFHT $H\alpha$ image shows more clearly the structure of the large star-forming complex around the ULX. The ring-like structure of the H II region (Figs 13 and 14) suggests that an expanding wave of star formation has recently moved from a centre (which appears to be near but not coincident with the ULX) outwards. Assuming a Salpeter IMF down to a lower mass limit of $1 M_{\odot}$, as explained in Section 4.3, we estimate from Starburst99 models (Leitherer et al. 1999) that continuous star formation over the last 30 Myr at a rate of $\sim 10^{-2}$ – $10^{-2.5} M_{\odot} \text{ yr}^{-1}$ (depending on the choice of metal abundance and upper mass limit) would account for the integrated luminosity ($M_B \approx -13.5$) and the observed number of O stars.⁵

This rate implies a mass in stars of ~ 1 – $3 \times 10^5 M_{\odot}$. The efficiency for the conversion of molecular gas into stars is generally $\lesssim 10$ per cent (e.g. Planesas, Colina & Perez-Olea 1997; Tan 2000). Moreover, some of the gas will be in atomic form; we have no observational data to determine the H I/H₂ ratio in this region, but we can assume for the sake of our order-of-magnitude calculation that they contribute in equal measure; we shall later see that this assumption is justified. Therefore, we estimate that the total mass (stars plus swept-up gas) in this complex is at least a few $10^6 M_{\odot}$.

On the other hand, we can also place an upper limit on the total mass in the region. We see from the *XMM-Newton* Optical Monitor (OM) image (Fig. 1) that it is located just outside the star-forming region in the disc of NGC 4559. This suggests that, before the triggering event, the local surface density was just below the threshold necessary for the onset of gravitational collapse and star formation. There are two empirical thresholds for star formation (Elmegreen 2002 and references therein). A constant-density threshold (more often applied to dwarf and irregular galaxies) requires a total surface density $\Sigma_g > \Sigma_{\text{min}} \approx 6 M_{\odot} \text{ pc}^{-2}$. Alternatively, a variable threshold based on Toomre's stability criterion (Toomre 1964) is more often applied to spiral galaxies:

$$\Sigma_g > \Sigma_{\text{min}} \approx \alpha \frac{\kappa \sigma}{\pi G}$$

where $\alpha \approx 0.7$ is an empirical constant, σ is the velocity dispersion of the gas, $\kappa = (2)^{0.5} (V/R)(1 + dV/dR)^{0.5}$ is the epicyclic frequency at radial distance R and V is the circular velocity of the galaxy at radius R (e.g. Kennicutt 1989, 1998; Wong & Blitz 2002; Boissier et al. 2003). We can estimate $V(R)$ in NGC 4559 from the Westerbork observations of neutral Hydrogen in Irregular and Spiral galaxies (WHISP) Survey⁶ 21-cm H I radio observations: at a distance $R = 16$ kpc, the velocity curve is flat, with an asymptotic velocity $V \approx 110 \pm$

⁵ If we assume a cut-off of the Salpeter IMF at $0.1 M_{\odot}$ instead, the inferred star formation rate (SFR) is $\sim 10^{-1.5}$ – $10^{-2} M_{\odot} \text{ yr}^{-1}$.

⁶ <http://www.astro.rug.nl/~whisp/>

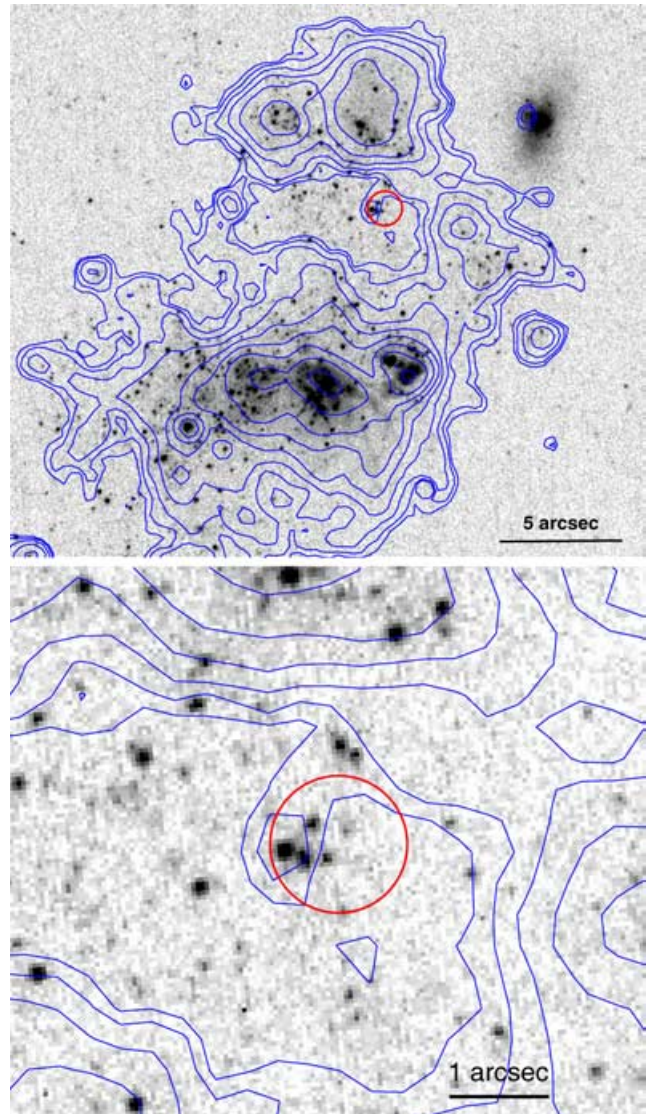


Figure 14. The ULX is located inside, although not at the centre, of a large ring-like H II region. Greyscale image: *HST* WFPC2 (PC chip), f450w filter ($\approx B$). Contours: $H\alpha$ image from the 3.6-m CFHT. We speculate that the dwarf galaxy seen at the north-west corner of the field is responsible for triggering this expanding wave of star formation, as it plunged through the gas-rich outer disc of NGC 4559 some 30 Myr ago.

5 km s^{-1} . The gas velocity dispersion ≈ 5 – 10 km s^{-1} (Boissier et al. 2003); a value commonly used is $\sigma = 6 \text{ km s}^{-1}$, following Kennicutt (1989). Hence, the Toomre criterion implies a local surface density $\Sigma_g < \Sigma_{\text{min}} \approx 4$ – $7 M_{\odot} \text{ pc}^{-2}$ before the onset of star formation, 30 Myr ago; this is in agreement with the threshold estimated from the constant-density criterion.

The star-forming complex has a projected area on the sky of $\approx 300 \text{ arcsec}^2$. Considering the viewing angle, this corresponds to a physical area of $\approx 1.8 \times 10^6 \text{ pc}^2$. From this, we can estimate that the total mass (essentially, atomic and molecular gas) contained in that region before the triggering of star formation was $< 10^7 M_{\odot}$. Combining this upper limit with the lower limit derived earlier, we can conclude that the star-forming complex contains a total mass ≈ 5 – $10 \times 10^6 M_{\odot}$.

We speculate that an initial perturbation caused a local increase in the gas density, triggering an expanding wave of star formation.

Considering the average SFR estimated earlier and the size of the ring where star formation has taken place, we can use a relation in Kennicutt (1998, see in particular, his fig. 6) to estimate the gas density in the ring: we infer that $\Sigma \approx 10\text{--}20 M_{\odot} \text{pc}^{-2}$. Therefore, a small density perturbation, by a factor ≈ 2 , would have sufficed to trigger the star-forming event.

As an aside, we note that these values of the total gas surface density correspond to a pressure $\log(P/k_B) \approx 3.5\text{--}4$ (where P/k_B is expressed in $\text{cm}^{-3} \text{K}$) at the disc mid-plane, which in turns corresponds to a regime where molecular and atomic hydrogen give a similar contribution to the total gas mass (Wong & Blitz 2002). This is consistent with our earlier assumption.

5.2 H α luminosity

Having estimated the total SFR of the complex, we can re-examine the CFHT H α image, recalling the relation between SFR and H α luminosity in star-forming galaxies, namely $L_{\text{H}\alpha} (\text{erg s}^{-1}) \approx 10^{41.3 \pm 0.2} \text{SFR} (M_{\odot} \text{yr}^{-1})$ (Kennicutt 1998; Buat et al. 2002). We expect an H α luminosity $\approx 10^{39} \text{erg s}^{-1}$ for the whole complex, neglecting the effect of extinction for this order-of-magnitude calculation.

Alternatively, from our previous estimate of the total mass in the star-forming complex, and the size of the H α -emitting ring, we estimate a baryon number density $\sim 1 \text{cm}^{-3}$ in that ring. This estimate can only be accurate to an order of magnitude, because we ignore the real geometry and vertical extent of that region. Assuming that H α comes from Case B recombinations in a gas at $T \approx 10000 \text{K}$ (typical of warm interstellar medium), we can determine the emission coefficient $j_{\text{H}\alpha}$ and the luminosity $L_{\text{H}\alpha} \approx 4\pi j_{\text{H}\alpha}$. We have $4\pi j_{\text{H}\alpha}/(N_p N_e) \approx 3 \times 10^{-25} \text{erg s}^{-1} \text{cm}^3$ (Osterbrock 1989). This value is only weakly dependent on the temperature, changing by a factor of 3 over the 5000–201 000 K temperature range. Integrated over a characteristic scale $\sim (500 \text{pc})^3$, this implies a total H α luminosity $\sim 10^{39} \text{erg s}^{-1}$, consistent with our previous estimate.

Using this value as a calibration for the total observed count rate in the image, we can then estimate an H α luminosity $\approx 1\text{--}3 \times 10^{35} \text{erg s}^{-1}$ for the optical counterpart of the ULX. We stress that this is only an order-of-magnitude estimate, given the large number of assumptions on which it is based. We will carry out a more accurate study of the optical continuum and H α emission with the *HST* ACS, next year.

As discussed earlier, a small group of O and early-type B stars is located at the ULX position. Are they the Balmer line sources seen in the CFHT image? H α emission is often detected from the excretion disc or envelope around Oe/Be stars: the brightest systems have a luminosity $\approx 2\text{--}4 \times 10^{34} \text{erg s}^{-1}$ (Janot-Pacheco, Motch & Pakull 1988; Apparao 1998; Stevens, Coe & Buckley 1999), still a few times fainter than observed at the X-7 position in NGC 4559. OB supergiants are another source of Balmer emission: the H α line emission is proportional to the mass-loss rate in the stellar wind and can reach luminosities $\approx 7 \times 10^{34} \text{erg s}^{-1}$ for stars with a mass-loss rate of $\approx 10^{-5.4} M_{\odot} \text{yr}^{-1}$ (Klein & Castor 1978; Ebbets 1982). Colliding winds in O-type close binary systems are also a source of Balmer emission: typical luminosities are \sim a few $\times 10^{34} \text{erg s}^{-1}$ (Thaller et al. 2001). We conclude that these mechanisms are probably too faint to explain the observed H α flux at the ULX position.

None of the previous scenarios requires the presence of an accreting compact object. However, a compact object may provide additional mechanisms for H α emission. Line emission is usually detected from accretion discs in low-mass X-ray binaries; however, characteristic luminosities are generally much lower, for example,

$L_{\text{H}\alpha} \sim$ a few $\times 10^{31} \text{erg s}^{-1}$ for the BH candidate *GRO* 1955–40 during the 1996 June high/soft state (Soria, Wu & Hunstead 2000). Stronger emission is seen from the high-mass X-ray binary Cyg X-1, where $L_{\text{H}\alpha} \approx 2 \times 10^{33} \text{erg s}^{-1}$ in the high/soft state (Tarasov et al. 2003). For higher values of the mass transfer rate, close or above the Eddington accretion rate, a strong radiatively driven wind is likely to be formed from the accretion disc surface, resulting in an optically thick envelope or outflow enshrouding the X-ray source (Shakura & Sunyaev 1973). For example, the intermediate-mass X-ray binary V4641 Sgr shows strong H α emission ($L_{\text{H}\alpha} \approx 4 \times 10^{34} \text{erg s}^{-1}$ during a short phase of super-Eddington accretion (Revnivtsev et al. 2002a,b; Chaty et al. 2003). This is still less than that observed near the ULX position.

Even stronger Balmer line emission is found in the BH candidate SS 433, a system for which persistent super-Eddington accretion has been invoked: the luminosity in the stationary H α component (thought to be mostly associated with the inner accretion disc and its envelope) is $L_{\text{H}\alpha} \sim 10^{36} \text{erg s}^{-1}$ (Asadullaev et al. 1983). Super-Eddington accretion on to a stellar-mass BH, with the formation of strong radiatively driven disc winds and outflows, is a possible explanation for ULXs with X-ray luminosities up to $\approx 10^{40} \text{erg s}^{-1}$ observed in star-forming environments (King 2002, 2003). It was also suggested that the soft thermal component at $kT \sim 0.1 \text{keV}$ often seen in those systems (including NGC 4559 X-7, Paper I) may come from the down-scattering of harder X-ray photons in the outflow (King & Pounds 2003).

Another possibility is that the H α emission comes from X-ray ionized clouds around the ULX, a scenario similar to that found in Seyfert galaxies. We shall estimate the order-of-magnitude H α luminosity expected from X-ray ionized gas in the next section. In any case, future studies of the H α emission from the X7 counterpart may reveal more clues on the nature of this X-ray source. In particular, variations in the H α emission associated with X-ray state transitions would provide a significant test for the size, geometry and true luminosity of the system.

5.3 An X-ray ionized nebula?

In addition to a possible point-like counterpart, we should also consider whether the ULX contributes to the ionization of the larger ring-like structure. Emission nebulae with sizes of a few hundred parsecs, showing both low and high ionization lines, with $L_{\text{H}\alpha} \sim$ a few $\times 10^{37}\text{--}10^{38} \text{erg s}^{-1}$, have been found around many nearby ULXs, for example NGC 1313 X-1 and X-2, M 81 X-9 and Holmberg II X-1 (Pakull & Mirioni 2002; Wang 2002). Some of these nebulae have been shown to be X-ray photoionized by the ULX. On a smaller scale (size of a few parsecs, $L_{\text{H}\alpha} \approx 10^{37} \text{erg s}^{-1}$), an X-ray photoionized emission nebula was found around the BH candidate LMC X-1 (Pakull & Angebault 1986).

Extrapolating the X-ray spectral fits presented in Paper I, we can estimate the number of photons of energy $> 13.6 \text{eV}$ intercepted by the gas surrounding the X-ray source (i.e. not including the line-of-sight foreground absorption), assuming that the emission is isotropic. Blackbody plus power-law models give the highest number of ionizing photons ($\approx 3 \times 10^{49} \text{s}^{-1}$); however, this is almost certainly an upper limit, because the power-law component is likely to be truncated at low energies. Comptonization models such as BMC in XSPEC may provide a more physical estimate: in this class of models, the power-law component does not extend below the seed thermal component at $kT \approx 0.1 \text{keV}$. Using the bmc fit to the *XMM-Newton* spectrum (Paper I), we estimate $\approx 10^{49}$ ionizing

photons s^{-1} from the ULX, intercepted by the surrounding nebula along our line of sight. The absorption in the NGC 4559 Galactic plane is likely to be higher; if all the X-ray flux were intercepted by the nebula there, it would approximately double the supply of hydrogen-ionizing photons, i.e. $\approx 2 \times 10^{49}$ photons s^{-1} using the bmc spectral model.

The number of $H\alpha$ photons emitted as a consequence of this ionizing flux is given by:

$$\begin{aligned} \frac{L_{H\alpha}}{h\nu_{H\alpha}} &\approx \frac{\alpha_{H\alpha}^{\text{eff}}(H^0, T)}{\alpha_B(H^0, T)} \int_{13.6\text{eV}}^{\infty} \frac{L_\epsilon}{\epsilon} [1 - \exp(-\tau_\epsilon)] d\epsilon \\ &\approx \frac{\alpha_{H\alpha}^{\text{eff}}}{\alpha_B} \times (1-3) 10^{49} s^{-1}, \end{aligned}$$

where τ_ϵ is the total optical depth in the nebula at energy ϵ , $\alpha_{H\alpha}^{\text{eff}}(H^0, T)$ is the effective recombination coefficient for the $H\alpha$ line and $\alpha_B(H^0, T)$ is the recombination coefficient summed over all levels above the ground state (Pakull & Angebault 1986 and references therein). The ratio of the recombination coefficients is only weakly dependent on the gas temperature; using typical values from Osterbrock (1989), we obtain an $H\alpha$ line emission of $\approx (3-10) \times 10^{48}$ photons s^{-1} , i.e. a luminosity $\approx (1-3) \times 10^{37}$ erg s^{-1} . This is much less than the total $H\alpha$ luminosity estimated earlier, for the whole star-forming ring. We conclude that the X-ray flux from the ULX does not significantly contribute to the Balmer line emission of the large surrounding H II region. However, it may explain the point-like emission seen within the ULX error circle, as discussed in the previous subsection.

Detection of He II $\lambda 4686$ line emission would provide a much more stringent test for the presence of X-ray photoionized gas around the ULX: this is because even the hottest O stars do not provide enough photons with energies > 54 eV, required to produce doubly ionized Helium. Measurements of high [O I] $\lambda 6300/H\alpha$ and [O III] $\lambda 5007/H\beta$ emission line ratios would be another test for the X-ray photoionization scenario (Pakull & Mirioni 2002). We are planning to conduct new spectroscopic observations of the field, to investigate this issue.

5.4 What triggered the expanding wave of star formation?

If we interpret the complex as an expanding star formation front, an important question to address is what the relation is between the ULX and the surrounding H II region. Large, isolated shell- or ring-like star-forming complexes of comparable size (500–1000 pc) and age (10–30 Myr) have been found in other nearby spiral galaxies: for example in NGC 6946 (Larsen et al. 2002) and, on a smaller scale, in M 83 (Comerón 2001). Gould’s belt in the Milky Way is also similar. The star-forming complex in NGC 4559 is a factor of 2 brighter than Gould’s belt and a factor of 4 fainter than the NGC 6946 complex. The latter has a young superstar cluster at its centre, while Gould’s belt and the complex in M 83 contain only OB associations. None of them contains a ULX, unlike the star-forming complex in NGC 4559. This suggests that the ULX is a side effect, rather than the determinant factor for the triggering and subsequent evolution of the star-forming episode.

Possible explanations for the initial triggering of such complexes are (Elmegreen, Efremov & Larsen 2000; Larsen et al. 2002): the collapse of a supergiant molecular cloud at the end of a spiral arm; a supernova explosion (which in our case might also have been the progenitor of NGC 4559 X7); or the infall of a high-velocity H I cloud or satellite galaxy through the outer Galactic disc. In all cases, the initial perturbation creates a radially expanding density

wave or ionization front, which sweeps up the neutral interstellar medium. Clustered star formation along the expanding bubble rim is triggered by the gravitational collapse of the swept-up material (e.g. Elmegreen & Lada 1977; Whitworth et al. 1994).

The large size of the complex in NGC 4559, its location in the outer disc, the lack of other star-forming regions nearby and the absence of diffuse X-ray emitting gas inside the star-forming complex seem to favour the collision hypothesis over the supernova model (Tenorio-Tagle et al. 1986, 1987). The impact of an $\approx 3 \times 10^5 M_\odot$ H I cloud on the Milky Way disc was simulated (Comerón & Torra 1994) to explain the formation of Gould’s belt. They show that, after ≈ 30 Myr, the mass of the cold swept-up material is comparable or larger than the mass of the impacting cloud. Similar consequences would come from the passage of a globular cluster ($M \sim 10^6 M_\odot$) through a gas-rich disc (Wallin, Higdon & Staveley-Smith 1996). In that case, the perturbation imparted by the colliding object to the disc gas would be entirely gravitational. A proper motion study of the Milky Way globular cluster NGC 6397 (Rees & Cudworth 2003) found that the cluster passed through the Galactic disc $\lesssim 5$ Myr ago and may have dynamically triggered the formation of the young open cluster NGC 6231.

5.5 A dwarf galaxy plunging through the disc?

An intriguing result of our optical study of the X7 environment is that we do indeed see an object that could have plunged through the gas-rich disc of NGC 4559, triggering the expanding density wave. The culprit could be the yellow galaxy located ≈ 7 arcsec (projected distance of 340 pc) north-west of the ULX (Figs 2, 14 and 15). This object cannot be a large background elliptical galaxy, because its isophotes are too irregular (Fig. 15). Its shape, size and luminosity are consistent with a dwarf irregular (or, possibly, a tidally disturbed dwarf elliptical) at approximately the same distance as NGC 4559 (Sandage & Binggeli 1984). We cannot presently rule out the possibility that it is a chance line-of-sight coincidence, but we suggest that the most natural interpretation is a small satellite galaxy of NGC 4559. Existing 21-cm H I radio observations (e.g., the WHISP survey) do not show any large-scale velocity distortions, but the satellite dwarf is perhaps too small to influence the global galactic kinematics significantly. However, as it crossed the disc, it would have significantly perturbed the local gas density, both hydrodynamically (ram pressure) and dynamically (gravitational perturbation). A dIrr galaxy contains both gas and dark matter, hence its impact would have been even more significant than that of a globular cluster. We are planning optical spectroscopic observations to determine the kinematics and distance of the dwarf galaxy, and therefore test this hypothesis.

If the dIrr galaxy is indeed physically associated with the star-forming complex, its integrated absolute brightness is $M_B \approx -10.7$, with observed colour indices $B - V \approx 0.47$ and $V - I \approx 0.73$. These colours are typical of a population dominated by F5–F8 MS stars, suggesting an old age. Assuming a single burst of star formation, we infer (using Starburst99, Leitherer et al. 1999) a visible stellar mass of $\sim 10^6 M_\odot$ for the galaxy and an age $\gtrsim 10^9$ yr for the dominant component of its stellar population.

As a comparison, this candidate satellite galaxy would be somewhat similar to the faint dwarf irregular galaxy Camelopardalis B (Cam B) in the IC 342/Maffei group, which has $M_B \approx -10.9$, $B - V \approx 0.6$ (Begum, Chengalur & Hopp 2003). The stellar mass in Cam B is estimated to be $\approx 3.5 \times 10^6 M_\odot$ and the total gas mass $\approx 6.6 \times 10^6 M_\odot$; the total dynamical mass is $\approx 1.1 \times 10^8 M_\odot$, hence the galaxy is strongly dark-matter dominated (Begum et al. 2003).

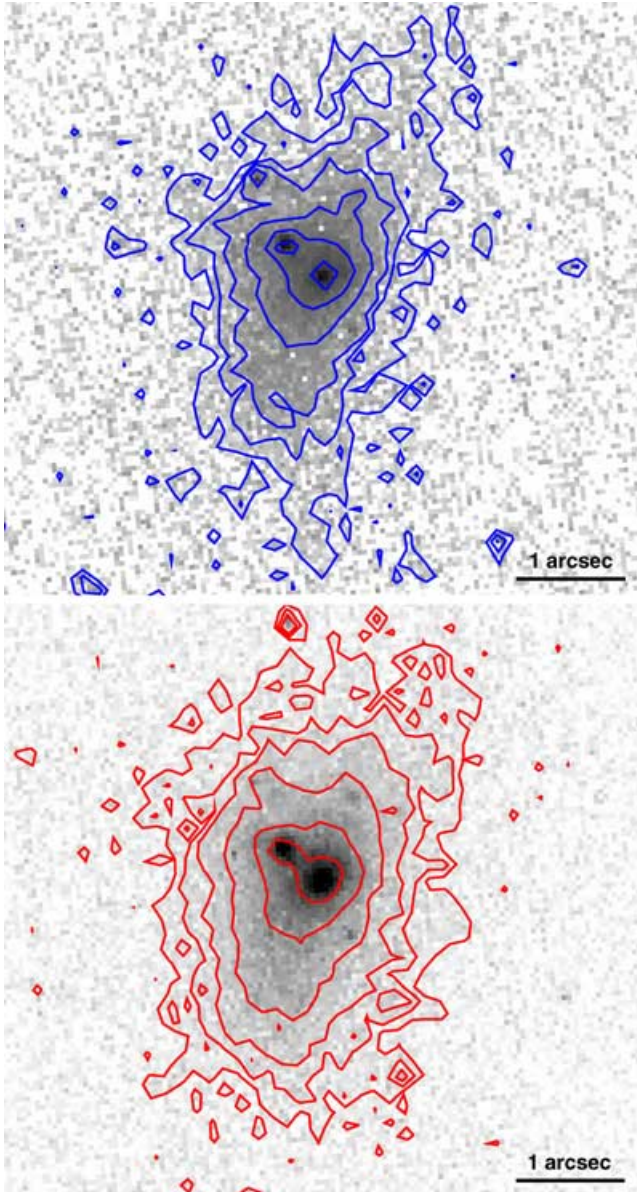


Figure 15. Close-up images of the candidate satellite galaxy, from the *HST* WFPC2 images. Top panel: image in the f450w filter. Bottom panel: image in the f814w filter. Both sets of contours are in a logarithmic scale, with arbitrary zero-point.

In fact, dark matter density dominates over stellar and gas density even in the inner regions.

5.6 Star formation induced by the colliding satellite?

In addition to the old stellar component, the candidate satellite galaxy near NGC 4559 shows two bright clusters and a few more, much fainter lumps. The two brightest clusters have luminosities $M_B \approx -7.2$ and $M_B \approx -7.1$, and colours consistent with an age $\sim 10^7$ yr and masses of \sim a few $\times 10^3 M_\odot$. Their brightness and morphology is consistent with the star-forming complexes often found in dIrr galaxies (Parodi & Binggeli 2003). We obtain that the percentage of flux in the B band as a result of these star-forming complexes (lumpiness index) is ≈ 7 per cent of the total B -band flux, the same value found for a large sample of irregulars and spirals regard-

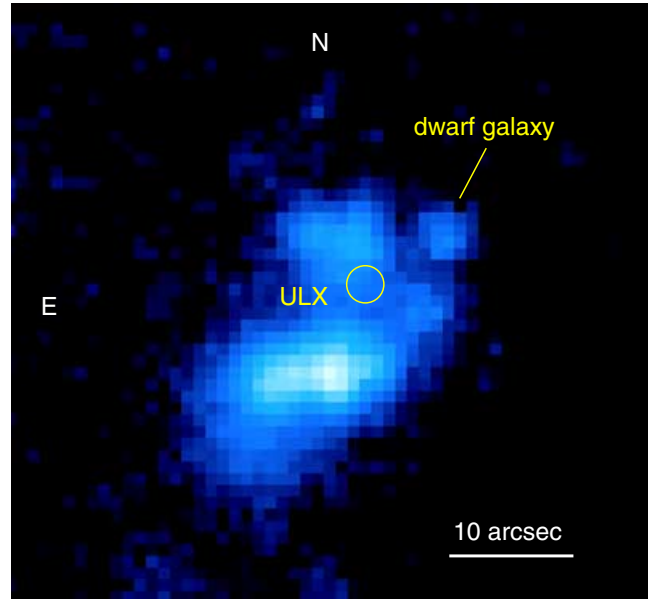


Figure 16. The dwarf galaxy near the X7 ULX is detected in the *XMM-Newton* Optical Monitor (OM) image (UVW1 filter). This is evidence of recent (but not current: cf. the $H\alpha$ image, Figs 13 and 14), moderate star formation.

less of Hubble type and galactic mass (Elmegreen & Salzer 1999; Parodi & Binggeli 2003). Thus, the lumpiness index is thought to be a measure of star formation efficiency. These considerations support the idea that the bright lumps are indeed clusters in the dIrr satellite galaxy and not simply background or foreground stars in NGC 4559. The dwarf galaxy is also detected in the *XMM-Newton* OM image (Fig. 16), taken in the UVW1 filter ($\approx 2500\text{--}3500 \text{ \AA}$). This also indicates recent star formation, in addition to the old stellar population, which would not be detected in the near-UV. (On the other hand, the $H\alpha$ image, Fig. 13, shows that the current SFR is negligible). The OM count rate is $0.115 \pm 0.005 \text{ ct s}^{-1}$: if we assume that the colours of the younger population are typical of a B0V star, such a count rate in the UVW1 filter corresponds to $M_B \approx -7.9 \pm 0.1$, in agreement with the *HST* WFPC2 observations.

It is possible that this small, later episode of star formation in the dIrr galaxy may also have been triggered when this small satellite passed through the disc of NGC 4559. If so, the younger stars may have been formed either from gas left in the dwarf galaxy, or collected into its gravitational potential well as it passed through the gas-rich disc. The non-spherical appearance of the large star-forming complex in NGC 4559 may be the result of an oblique impact, possibly from the south-east to the north-west direction. The projected distance of the dIrr from the centre of the star-forming ring is ≈ 400 pc, corresponding to a projected relative velocity of $\approx 15 \text{ km s}^{-1}$ over 30 Myr; however, this is certainly a lower limit, because we have no elements to estimate the velocity component along the line of sight.

Thus, we could view the star-forming complex in NGC 4559 as a small-scale version of the Cartwheel galaxy, where many young ULXs have been detected in the expanding, star-forming ring (Gao et al. 2003). In the Cartwheel, the initial perturbation causing the expanding density wave is entirely the result of the gravitational interaction between the two galaxies; in the case of NGC 4559, it may be the result of both the dynamical impulse and the direct hydrodynamical interaction between the gas in the satellite and in

the disc. A more detailed analysis of this possibility is left to a separate work.

6 ENVIRONMENTAL CONDITIONS FAVOURABLE TO ULX FORMATION

NGC 4559 X7 offers an example of a bright ($L_x > 2 \times 10^{40}$ erg s^{-1}) ULX in a low-metallicity, actively star-forming environment disturbed by close galaxy interactions. At least one and often all of these elements seem to be a common feature for many of the galaxies hosting ULXs: for example, galactic interactions and high SFRs for the Antennae (Zezas et al. 2002; Fabbiano et al. 2003), the Cartwheel ring (Gao et al. 2003), M 82 (Griffiths et al. 2000), the Mice (Read 2003), NGC 7714/15 (Soria & Motch 2004); low metal abundance for the Cartwheel ring, NGC 7714/15, the M 81 group dwarfs (Makarova et al. 2002; Wang 2002) and a group of nearby blue compact dwarfs including I Zw 18 (Thuan et al. 2004). A preferential association between ULXs and interacting galaxies was shown in Swartz et al. (2004); a connection between ULX formation and low- Z environments was suggested in Pakull & Mirioni (2002).

This leads us to speculate that these two environmental conditions may be particularly favourable for producing massive remnants. For example, galaxy mergers, close interactions and collisions with satellite galaxies or high-velocity H I clouds favour clustered star formation. The core of young star clusters is an environment where intermediate-mass BHs (with masses up to $\sim 1000 M_\odot$) may be formed, through the Spitzer instability, runaway core collapse and merger of the O stars (Portegies & McMillan 2002; Gürkan, Freitag & Rasio 2004; Portegies et al. 2004; Rasio, Freitag & Gürkan 2004). One of the open questions (Portegies et al. 2004) is what range of cluster masses and radii offers the best chance for the core collapse/stellar coalescence process to occur within the lifetime of its more massive O stars (≈ 3 Myr). However, we have found that this ULX in NGC 4559 is not located in or near a bright cluster: hence, this formation channel seems unlikely for this object, unless the parent cluster has already dispersed. The tidal disruption of a massive parent cluster on a time-scale < 30 Myr is also unlikely.⁷

On the other hand, low metal abundance may, in principle, have an effect at at least two different stages: by allowing the formation of more massive progenitor stars; and by helping the formation of a more massive compact object from a normal progenitor star. The first of these effects is usually invoked to predict the formation of massive Population III stars (and, subsequently, of intermediate-mass BH remnants) at high redshift (Madau & Rees 2001). For metal abundances $Z \lesssim 10^{-4}$, molecular hydrogen is the only effective coolant in dense cloud cores. The cloud temperature cannot decrease below \sim a few 10^2 K regardless of density and the Jeans mass remains \sim a few $10^2 M_\odot$ at all stages. Thus, a dense clump will collapse into a single, very massive star (Bromm 2004 and references therein) without further subfragmentation. This simple mechanism does not work for SMC-type metal abundances such as those found

in NGC 4559 and in other nearby metal-poor dwarf galaxies with ULXs. It is also highly unlikely that zero-metallicity gas could still be present in the outskirts of those galaxies. However, it is possible that other mechanisms may lead to the same effect, making the cooling time-scale longer than the dynamical time-scale (time-scale for collapse) and therefore reducing the fragmentation during the cloud collapse. For example, we may speculate that a combination of reduced metal abundance and external heating of the cloud cores during the galaxy collision process (through shocks and turbulence) might lead to the formation of more massive stars and remnants. The balance of heating and cooling in a molecular cloud core can be approximately expressed through a polytropic equation of state, $P = K \rho^\gamma$. It was suggested (Spaans & Silk 2000; Li, Klessen & Mac Low 2003) that a stiff polytropic index $\gamma > 1$ should reduce or suppress fragmentation during the molecular core collapse, leading to the formation of more massive stars. This naturally occurs in a gas with primordial metal abundances, but it may also occur at higher metallicities ($Z > 0.1 Z_\odot$) for example if the gas is irradiated by an infrared (IR) background ($T \sim 100$ K; Spaans & Silk 2000).

The effect of low metal abundance on the evolution of normal early-type stars is to reduce the mass-loss rate in the radiatively driven wind ($\dot{M}_w \sim Z^{0.85}$; Vink, de Koter & Lamers 2001; see also Bouret et al. 2003). This leads to a more massive stellar core, which may then collapse into a more massive BH, via normal stellar evolution. Hence, low abundances may explain the formation of isolated BHs with masses up to $\approx 50 M_\odot$ (i.e. up to approximately half of the mass of the progenitor star) and isotropic Eddington luminosities $\approx 7 \times 10^{39}$ erg s^{-1} . Two-dimensional hydrodynamic simulations of core collapse in massive stars by Fryer (1999) and Fryer & Kalogera (2001) found that they could not produce BH remnants more massive than $\approx 20 M_\odot$. However, they did not rule out the possibility of higher BH masses formed from stellar progenitors more massive than $\approx 40 M_\odot$ if wind losses are negligible.

7 MASS OF THE ACCRETING BH

Based on the previous qualitative arguments, if accreting BHs with masses ~ 50 – $100 M_\odot$ (more massive than those found in Milky Way X-ray binaries) can indeed be formed from stellar evolution processes, they would be natural candidates to explain most ULXs, up to isotropic luminosities $\approx 10^{40}$ erg s^{-1} , without additional assumptions on the geometry of emission. However, NGC 4559 X7 has an isotropic luminosity persistently $\gtrsim 2 \times 10^{40}$ erg, s^{-1} in the 0.3–10-keV band and an extrapolated bolometric luminosity $> 5 \times 10^{40}$ erg s^{-1} (Paper I): hence, it may still be too bright to be a normal stellar-mass remnant, if we assume strictly Eddington-limited isotropic emission. Therefore, we are left with three alternatives for this source. A normal stellar-mass BH ($M \lesssim 20 M_\odot$) would require either strong, collimated beaming (it would effectively be a microblazar) or strongly super-Eddington emission. An ~ 50 – $100 M_\odot$ BH accreting from a 15–25 M_\odot supergiant companion would require only mildly anisotropic emission (geometrical beaming of a factor ~ 5 – 10 ; King 2004) or mildly super-Eddington luminosity. An intermediate-mass BH ($M \gtrsim 500 M_\odot$) would allow for isotropic, sub-Eddington emission.

The X-ray spectral data (Paper I) show the presence of a very soft thermal component ($kT_{in} \approx 0.12$ – 0.15 keV); if fitted with a standard disc-blackbody model truncated at the Schwarzschild innermost stable orbit, its luminosity and temperature together suggest a mass $\approx 1000 M_\odot$. It has been suggested (King & Pounds 2003) that the very soft thermal component seen in this and other ULXs may not be an indicator of the inner-disc temperature, but may instead

⁷ Clusters with an initial (embedded) mass between \sim a few $\times 10^3$ and \sim a few $\times 10^4 M_\odot$ do get disrupted on a shorter time-scale because of explosive gas losses (Kroupa & Boily 2002); however, in that case the dispersal occurs on a time-scale $\tau \lesssim t_{cr} \approx 10^{-3} t_{th} \ll t_{cc} \approx 10^{-1} t_{th}$, where t_{cr} is the crossing time-scale, t_{cc} is the core-collapse time-scale and t_{th} is the relaxation time-scale (Spitzer 1987). In other words, the disruption would occur before there is enough time for the core to collapse. Moreover, the mass of the collapsed core is found to be $\sim 10^{-3}$ times the total cluster mass (Gürkan et al. 2004); hence, clusters in this mass range would probably not be able to produce BHs more massive than $\sim 50 M_\odot$.

be the result of photon down-scattering in an optically thick outflow shrouding the central X-ray source. This radiatively driven outflow would be more likely for X-ray sources emitting close or above the Eddington limit. If we accept this argument, we cannot rule out the alternative interpretation of this system as a $\sim 50\text{--}100 M_{\odot}$ BH, with Eddington or mildly super-Eddington emission and perhaps mildly anisotropic emission (gaining a factor $\lesssim 10$ in the observed flux from the combination of the two effects). On the other hand, Miller, Fabian & Miller (2004) argue that the presence of a power-law hard component of similar luminosity ($\sim 10^{40}$ erg s $^{-1}$) to that of the soft thermal component requires a BH with mass $\sim 1000 M_{\odot}$. The X-ray timing data (Paper I) suggest the presence of a break in the power density spectrum at ≈ 0.03 Hz; this can indicate either a BH mass $\approx 40 M_{\odot}$ or $\approx 1000 M_{\odot}$, depending on the identification of the break in comparison with standard power density spectra of X-ray binaries and AGN. In any case, we can conclude that these X-ray findings are not consistent with a low-mass, relativistically beamed microblazar scenario and suggest a BH mass $\gtrsim 50 M_{\odot}$. (See also Davis & Mushotzky 2004 for a more general argument against strong beaming.)

The optical data indicate an association with a young region of massive star formation at the edge of the Galactic disc (age < 30 Myr). They also rule out an association between the ULX and massive star clusters; hence, they rule out at least one mechanism of formation for an intermediate-mass BH. Other formation processes have been proposed for such objects: e.g. from Population III stars. However, in this case, rather contrived hypotheses would be required to explain its location in a young star-forming complex on the Galactic disc plane and the capture of a companion star. Therefore, on balance, the optical data are more consistent with a BH originating in the recent episode of massive star formation and accreting from an OB companion.

A possible counterargument against the existence of a $\sim 50\text{--}100 M_{\odot}$ BH in this field is that it would require a progenitor star at least twice as massive; yet, all the stars we see today are consistent with normal OB stars and there are no extraordinarily bright stellar objects. This may be the case if the peculiar physical conditions in the molecular gas that led to the formation of very massive stars were present only for a short time at the beginning of the star-forming episode, when the perturbation was stronger. All the very massive stars formed at the time have already died and star formation proceeds today in a more conventional way, while the density wave expands and weakens. Another possibility is that, if such massive stars still exist today in this field, we may have mistaken them for star clusters. For example, we cannot rule out that the bright ($M_V \approx -9.5$), unresolved source described as a cluster in Section 4.4 might instead be a very massive star. In conclusion, we argue that a young $\sim 50\text{--}100 M_{\odot}$ BH formed from stellar evolution processes is consistent with both the optical and the X-ray data. A BH with a mass $\sim 1000 M_{\odot}$ would also be consistent with (and in some respects preferred by) the X-ray data, but much more difficult to reconcile with the optical results. Further multiband studies of this ULX (in particular, radio and IR) are necessary to constrain the mass of the BH.

8 CONCLUSIONS

We have used *HST* WFPC2 images in the *B*, *V*, *I* bands, an *XMM-Newton* OM image in the UV band and a ground-based $H\alpha$ image to study the star-forming complex around a bright ULX at the edge of the late-type spiral NGC 4559. We find that star formation in the kpc-size complex near the ULX has occurred mostly over the last

≈ 30 Myr and is still ongoing in the southern part of the complex. The ULX is co-located with a small group of OB stars, but is not located in the most active region of the star-forming complex. Also, it does not appear to be associated with any massive young clusters or any extraordinary massive star: the brightest point source in the *Chandra* error circle is consistent with a single BSG of mass $\approx 20 M_{\odot}$. A few other stars are resolved inside the error circle: mostly BSGs and RSGs with inferred masses $\approx 10\text{--}15 M_{\odot}$. The candidate donor stars near X7 are consistent with an age of ≈ 20 Myr, except for the brightest one, for which we estimate an age of ≈ 10 Myr if it is a single, isolated star. However, it is possible that this star appears brighter and younger than its real age because of the effect of X-ray irradiation, if it is the true optical counterpart. $H\alpha$ emission is also seen at the position of this star and may come from X-ray ionized gas around the ULX.

Regardless of which is the true counterpart, it is very likely that the NGC 4559 X7 ULX is a young system (age ≈ 20 Myr) with a high-mass donor. This is analogous to what is found for the few other ULXs with an identified optical counterpart (Liu et al. 2002, 2004; Zampieri et al. 2004). It is also likely (given its X-ray luminosity) that accretion occurs via Roche lobe overflow and that the accreting BH is more massive than the secondary star, unlike typical high-mass X-ray binaries in the Galaxy. This would imply that the orbit widens as mass is transferred, in the absence of other mechanisms to remove angular momentum from the system. We noted, qualitatively, that a supergiant donor may ensure a steady mass transfer rate, because its thermal equilibrium radius expands as its mass decreases (unlike what happens for MS stars). If the supergiant donor is massive enough ($\gtrsim 15 M_{\odot}$), it may have a transfer rate $\sim 10^{-5} M_{\odot} \text{ yr}^{-1}$ over its nuclear time-scale $\sim 10^6$ yr (in the supergiant phase), as required by the observed luminosity.

We cannot conclusively determine whether the accreting BH was formed via normal stellar evolution (perhaps favoured by the low-metallicity environment or by galaxy collision processes), or is instead an intermediate-mass BH created via another mechanism. However, given the Galactic disc location and the age of the local stellar population, a young BH associated with the recent episode of star formation appears much more likely than a primordial BH. Runaway core collapse in a young superstar cluster is one mechanism proposed for the formation of a young intermediate-mass BH in a starburst or star-forming region. However, our optical study does rule out this scenario for X7. The only medium-size ($M \approx 10^{4.2} M_{\odot}$), young (25 ± 5 Myr) cluster in the field is located at $\gtrsim 600$ pc from the ULX; this distance also rules out a direct connection via BH ejection. Further analysis of the *Chandra* data (see also Paper I) shows that there are no X-ray sources associated with this cluster and in fact no other sources in the whole X7 field, brighter than the ACIS-S 12-count detection limit, corresponding to $\approx 4 \times 10^{37}$ erg s $^{-1}$ for standard spectral models suitable to accreting sources. Based on the results of our X-ray and optical studies, we suggest that the X7 ULX is consistent with a $\sim 50\text{--}100 M_{\odot}$ BH recently formed from stellar evolution processes and accreting from an OB companion via Roche-lobe overflow.

We have also studied the general properties of the stellar population in the large star-forming complex around X7. Its stellar population is consistent with an average SFR $\sim 10^{-2}\text{--}10^{-2.5}$ over the last 30 Myr. The observed optical colours and the blue-to-red supergiant ratio suggest a low metal abundance: $0.2 \lesssim Z/Z_{\odot} \lesssim 0.4$ (using the Padua tracks), or $0.05 \lesssim Z/Z_{\odot} \lesssim 0.2$ (from the Geneva tracks). This is also consistent with the low abundance found for the absorbing medium towards the X7 ULX, from our *XMM-Newton* study (Table 1 and Paper I).

The star-forming complex has a ring-like appearance; it is only faintly connected to the outermost spiral arm of NGC 4559 (Fig. 1) and there are no other strongly star-forming regions nearby. This suggests that it is an expanding wave of star formation, triggered by an initial density perturbation, in a region where the gas was only marginally stable to gravitational collapse. Similar isolated, ring- or shell-like star-forming complexes have been seen in the Milky Way and in nearby galaxies. A central superstar cluster or hypernova could have provided the initial trigger. However, in this case we propose that the most likely trigger was a collision with a satellite dwarf galaxy punching through the gas-rich outer disc of NGC 4559. A candidate dwarf galaxy is indeed visible a few arcsec north-west of the complex (Fig. 2). It is dominated by an old stellar population (age $\gtrsim 10^9$ yr) with a few clumps of younger stars (age $\sim 10^7$ yr). With a stellar mass $\sim 10^6 M_{\odot}$ and (by analogy with similar dwarf galaxies) a dark matter mass 1 order of magnitude larger, it would have produced a strong density wave in the gas-rich outer disc of NGC 4559. We are planning optical spectroscopic studies of this object to determine whether it is indeed physically associated to NGC 4559 as we propose and, if so, to estimate the physical parameters of the collision.

We note that this system could be a scaled-down version of the Cartwheel system (Gao et al. 2003), where bright, short-lived ULXs have been produced in the expanding wave of star formation, triggered by the galaxy collision (King 2004). Colliding or tidally interacting systems, low-metallicity environments and perhaps a high rate of clustered star formation seem to provide favourable conditions for the formation of ULXs. We have briefly mentioned some possible effects.

Finally, we need to take into account the existence of another bright ($L_x \gtrsim 10^{40}$ erg s $^{-1}$) ULX in this galaxy, NGC 4559 X10, located in the inner Galactic disc (Fig. 1). A preliminary investigation of its optical environment (Paper I) did not reveal a young star-forming region or bright massive stars near X10. It is possible that X7 and X10 have different ages and have been formed via different physical mechanisms. Perhaps this comparison can also shed light on the difference between typical ULXs in star-forming and elliptical galaxies. A detailed study of the similarities and differences between the environments of these two ULXs is left to further work, which will be based on a new set of *HST* ACS observations scheduled for 2005 March (including an H α observation).

ACKNOWLEDGMENTS

We thank Doug Swartz, Helmut Jerjen, Christian Motch and Fred Rasio for useful discussions and suggestions. We also thank the referee (Tim Roberts) for his helpful comments. RS would have been supported by a Marie Curie fellowship, if its payment had not been more than a year overdue.

REFERENCES

Apparao K. M. V., 1998, *A&A*, 337, 721
 Asadullaev S. S., Aslanov A. A., Kornilov V. G., Cherepashchuk A. M., 1983, *SvAL*, 9, 282
 Begelman M. C., 2002, *ApJ*, 568, L97
 Begum A., Chengalur J. N., Hopp U., 2003, *New Astron.*, 8, 267
 Boissier S., Prantzos N., Boselli A., Gavazzi G., 2003, *MNRAS*, 346, 1215
 Bouret J.-C., Lanz T., Hillier D. J., Heap S. R., Hubeny I., Lennon D. J., Smith L. J., Evans C. J., 2003, *ApJ*, 595, 1182
 Bromm V., 2004, *PASP*, 116, 103
 Buat V., Boselli A., Gavazzi G., Bonfanti C., 2002, *A&A*, 383, 801

Chaty S., Charles P. A., Martí J., Mirabel I. F., Rodríguez L. F., Shahbaz T., 2003, *MNRAS*, 343, 169
 Colbert E. J. M., Mushotzky R. F., 1999, *ApJ*, 519, 89
 Comerón F., 2001, *A&A*, 365, 417
 Comerón F., Torra J., 1994, *A&A*, 281, 35
 Cropper M. S., Soria R., Mushotzky R. F., Wu K., Markwardt C. B., Pakull M., 2004, *MNRAS*, 349, 39 (Paper I)
 Davis D. S., Mushotzky R. F., 2004, *ApJ*, 604, 653
 Dickey J. M., Lockman F. J., 1990, *ARA&A*, 28, 215
 Dohm-Palmer R. C., Skillman E. D., 2002, *ApJ*, 123, 1433
 Dolphin A. E., 2000, *PASP*, 112, 1383
 Ebbets D., 1982, *ApJS*, 48, 399
 Eggleton P. P., 1983, *ApJ*, 268, 368
 Elmegreen B. G., 2002, *ApJ*, 577, 206
 Elmegreen B. G., Lada C. J., 1977, *ApJ*, 214, 725
 Elmegreen D. M., Salzer J. J., 1999, *AJ*, 117, 764
 Elmegreen B. G., Shadmehri M., 2003, *MNRAS*, 338, 817
 Elmegreen B. G., Efremov Y. N., Larsen S., 2000, *ApJ*, 535, 748
 Fabbiano G., Krauss M., Zezas A., Rots A., Neff S., 2003, *ApJ*, 598, 272
 Fabrika S., Mescheryakov A., 2001, in Schilizzi R. T., Vogel S. N., Paresce F., Elvis M. S., eds, *Proc. IAU Symp. 205, Galaxies and their Constituents at the Highest Angular Resolutions*. Astron. Soc. Pac., San Francisco, p. 268 (astro-ph/0103070)
 Fagotto F., Bressan A., Bertelli G., Chiosi C., 1994, *A&AS*, 105, 29
 Fioc M., Rocca-Volmerange B., 1997, *A&A*, 326, 950
 Fryer C. L., 1999, *ApJ*, 522, 413
 Fryer C. L., Kalogera V., 2001, *ApJ*, 554, 548
 Gao Y., Wang Q. D., Appleton P. N., Lucas R. A., 2003, *ApJ*, 596, L171
 Girardi L., Bertelli G., Bressan A., Chiosi C., Groenewegen M. A. T., Marigo P., Salasnich B., Weiss A., 2002, *A&A*, 391, 195
 Gonzaga S., 2002, *WFPC2 Data Analysis: a Tutorial*, version 3.0. STScI, Baltimore, MD, USA
 Griffiths R. E., Ptak A., Feigelson E. D., Garmire G., Townsley L., Brandt W. N., Sambruna R., Bregman J. N., 2000, *Sci*, 290, 1325
 Guo J. H., Li Y., 2002, *ApJ*, 565, 559
 Gürkan M. A., Freitag M., Rasio F. A., 2004, *ApJ*, 604, 632
 Holtzman J. et al., 1995, *PASP*, 107, 156
 Irwin J. A., Bregman J. N., Athey A. E., 2004, *ApJ*, 601, L143
 Janot-Pacheco E., Motch C., Pakull M. W., 1988, *A&A*, 202, 81
 Kaaret P., Ward M. J., Zezas A., 2004, *MNRAS*, 351, L83
 Kennicutt R. C. Jr., 1989, *ApJ*, 344, 685
 Kennicutt R. C. Jr., 1998, *ApJ*, 498, 541
 King A. R., 2002, *MNRAS*, 335, L13
 King A. R., 2003, *ApJ*, 596, L27
 King A. R., 2004, *MNRAS*, 347, L18
 King A. R., Pounds K. A., 2003, *MNRAS*, 345, 657
 King A. R., Davies M. B., Ward M. J., Fabbiano G., Elvis M., 2001, *ApJ*, 552, L109
 Klein R. I., Castor J. I., 1978, *ApJ*, 220, 902
 Körding E., Falcke H., Markoff S., 2002, *A&A*, 382, L13
 Kroupa P., 2001, *MNRAS*, 322, 231
 Kroupa P., 2002a, *Sci*, 295, 82
 Kroupa P., 2002b, in Grebel E., Brandner W., eds, *ASP Conf. Ser. Vol. 285, Modes of Star Formation*. Astron. Soc. Pac., San Francisco, p. 86 (astro-ph/0102155)
 Kroupa P., Boily C. M., 2002, *MNRAS*, 336, 1188
 Kroupa P., Tout C. A., Gilmore G., 1990, *MNRAS*, 244, 76
 Kroupa P., Tout C. A., Gilmore G., 1993, *MNRAS*, 262, 545
 Kuiper L., van Paradijs J., van der Klis M., 1988, *A&A*, 203, 79
 Langer N., Maeder A., 1995, *A&A*, 295, 68
 Larsen S. S., Efremov Y. N., Elmegreen B. G., Alfaro E. J., Battinelli P., Hodge P. W., Richtler T., 2002, *ApJ*, 567, 896
 Larson R. B., 1998, *MNRAS*, 301, L569
 Leitherer C. et al., 1999, *ApJS*, 123, 3
 Lejeune T., Buser R., 1999, in Hubeny I., Heap S., Cornett R., eds, *ASP Conf. Vol. 192, Spectrophotometric Dating of Stars and Galaxies*. Astron. Soc. Pac., San Francisco, p. 211 (astro-ph/9905336)
 Lejeune T., Schaerer D., 2001, *A&A*, 366, 538

- Li Y., Klessen R. S., Mac Low M.-M., 2003, *ApJ*, 592, 975
- Liu J.-F., Bregman J. N., Seitzer P., 2002, *ApJ*, 580, L31
- Liu J.-F., Bregman J. N., Seitzer P., 2004, *ApJ*, 602, 249
- McCraday N., Gilbert A. M., Graham J. R., 2003, *ApJ*, 596, 240
- Madau P., Rees M. J., 2001, *ApJ*, 551, L27
- Maeder A., Meynet G., 2001, *A&A*, 373, 555
- Makarova L. N. et al., 2002, *A&A*, 396, 473
- Masetti N., Foschini L., Ho L. C., Dadina M., Di Cocco G., Malaguti G., Palazzi E., 2003, *A&A*, 406, L27
- Meynet G., Maeder A., Schaller G., Schaerer D., Charbonnel C., 1994, *A&AS*, 103, 97
- Miller J. M., Fabian A. C., Miller M. C., 2004, *ApJ*, 607, 931
- Monet D. G. et al., 2003, *AJ*, 125, 984
- Newton I., 1687, *Philosophiae Naturalis Principia Mathematica*, Vol. 3, S. Pepys, London, p. 419
- Osterbrock D. E., 1989, *Astrophysics of Gaseous Nebulae and Active Galactic Nuclei*. University Science Books, Mill Valley, CA, USA
- Pakull M. W., Angebault L. P., 1986, *Nat*, 322, 511
- Pakull M. W., Mirioni L., 2002, in *Proc. Symp. New Visions of the X-ray Universe in the XMM–Newton and Chandra Era*. ESTEC, the Netherlands, in press (astro-ph/0202488)
- Parodi B. R., Binggeli B., 2003, *A&A*, 398, 501
- Planesas P., Colina L., Perez-Olea D., 1997, *A&A*, 325, 81
- Podsiadlowski P., 1992, *PASP*, 104, 717
- Podsiadlowski P., Rappaport S., Han Z., 2003, *MNRAS*, 341, 385
- Portegies Zwart S. F., McMillan S. L. W., 2002, *ApJ*, 576, 899
- Portegies Zwart S. F., Baumgardt H., Hut P., Makino J., McMillan S. L. W., 2004, *Nat*, 428, 724
- Rasio F. A., Freitag M., Gürkan M. A., 2004, in Ho L. C., ed. *Carnegie Observatories Astrophysics Series, Vol. 1, Coevolution of Black Holes and Galaxies*. Cambridge University Press, Cambridge, UK, p. 138
- Read A. M., 2003, *MNRAS*, 342, 715
- Rees R. F., Cudworth K. M., 2003, *American Astronomical Society Meeting*, 203, 10.06
- Revnivtsev M., Gilfanov M., Churazov E., Sunyaev R., 2002a, *A&A*, 391, 1013
- Revnivtsev M., Sunyaev R., Gilfanov M., Churazov E., 2002b, *A&A*, 385, 904
- Ritter H., 1988, *A&A*, 202, 93
- Roberts T. P., Goad M. R., Ward M. J., Warwick R. S., O'Brien P. T., Lira P., Hands A. D. P., 2001, *MNRAS*, 325, L7
- Roberts T. P., Goad M. R., Ward M. J., Warwick R. S., 2003, *MNRAS*, 342, 709
- Roberts T. P., Warwick R. S., Ward M. J., Goad M. R., 2004, *MNRAS*, 349, 1193 (also, Erratum: 1994, *MNRAS*, 350, 1536)
- Salasnich B., Bressan A., Chiosi C., 1999, *A&A*, 342, 131
- Salasnich B., Girardi L., Weiss A., Chiosi C., 2000, *A&A*, 361, 1023
- Sandage A., Binggeli B., 1984, *AJ*, 89, 919
- Sanders D. B., Mazzarella J. M., Kim D.-C., Surace J. A., Soifer B. T., 2003, *AJ*, 126, 1607
- Schlegel D. J., Finkbeiner D. P., Davis M., 1998, *ApJ*, 500, 525
- Shakura N. I., Sunyaev R. A., 1973, *A&A*, 24, 337
- Smith L. J., Gallagher J. S., 2001, *MNRAS*, 326, 1027
- Soria R., Motch C., 2004, *A&A*, 422, 915
- Soria R., Wu K., Hunstead R. W., 2000, *ApJ*, 539, 445
- Soria R., Wu K., Page M. J., Sakellou I., 2001, *A&A*, 365, 273
- Spaans M., Silk J., 2000, *ApJ*, 538, 115
- Spitzer L., 1987, *Dynamical Evolution of Globular Clusters*. Princeton Univ. Press, Princeton, NJ, USA
- Stevens J. B., Coe M. J., Buckley D. A. H., 1999, *MNRAS*, 309, 421
- Strohmayer T. E., Mushotzky R. F., 2003, *ApJ*, 586, L61
- Swartz D. A., Ghosh K. K., Tennant A. F., Wu K., 2004, *ApJS*, 154, 519
- Tan J. C., 2000, *ApJ*, 536, 173
- Tarasov A. E., Brocksopp C., Lyuty V. M., 2003, *A&A*, 402, 237
- Tenorio-Tagle G., Bodenheimer P., Rozyczka M., Franco J., 1986, *A&A*, 170, 107
- Tenorio-Tagle G., Franco J., Bodenheimer P., Rozyczka M., 1987, *A&A*, 179, 219
- Thaller M. L., Gies D. R., Fullerton A. W., Kaper L., Wiemker R., 2001, *ApJ*, 554, 1070
- Thuan T. X., Bauer F. E., Papaderos P., Izotov Y. I., 2004, *ApJ*, 606, 213
- Toomre A., 1964, *ApJ*, 139, 1217
- Tully R. B., 1988, *Nearby galaxies catalog*. Cambridge Univ. Press, Cambridge, UK
- Vanbeveren D., De Loore C., Van Rensbergen W., 1998, *A&AR*, 9, 63
- Vink J. S., de Koter A., Lamers H. J. G. L. M., 2001, *A&A*, 369, 574
- Vogler A., Pietsch W., Bertoldi F., 1997, *A&A*, 318, 768
- Wallin J. F., Higdon J. L., Staveley-Smith L., 1996, *ApJ*, 459, 555
- Wang Q. D., 2002, *MNRAS*, 332, 764
- Weisskopf M. C., Wu K., Tennant A. F., Swartz D. A., Ghosh K. K., 2004, *ApJ*, 605, 360
- Wellstein S., Langer N., Braun H., 2001, *A&A*, 369, 939
- Westera P., Lejeune T., Buser R., Cuisinier F., Bruzual G., 2002, *A&A*, 381, 524
- Whitworth A. P., Bhattal A. S., Chapman S. J., Disney M. J., Turner J. A., 1994, *A&A*, 290, 421
- Wong T., Blitz L., 2002, *ApJ*, 569, 157
- Wu K., 1997, in Wickramasinghe D. T., Bicknell G. V., Ferrario L., eds, *Proc. IAU Colloquium 163, ASP Conf. Ser. Vol. 121, Accretion Phenomena and Related Outflows*. Astron. Soc. Pac., San Francisco, p. 283
- Wu K., Soria R., Page M. J., Sakellou I., Kahn S. M., de Vries C. P., 2001, *A&A*, 365, 267
- Zampieri L., Mucciarelli P., Falomo R., Kaaret P., Di Stefano R., Turolla R., Chieregato M., Treves A., 2004, *ApJ*, 603, 523
- Zezas A., Fabbiano G., 2002, *ApJ*, 577, 726
- Zezas A., Fabbiano G., Rots A. H., Murray S. S., 2002, *ApJ*, 577, 710

This paper has been typeset from a $\text{T}_{\text{E}}\text{X}/\text{L}_{\text{A}}\text{T}_{\text{E}}\text{X}$ file prepared by the author.